Boundary layer structure characteristics under objective classification of persistent pollution weather types in the Beijing area

Zhaobin Sun[1], Xiujuan Zhao*[1], Ziming Li[2],Guiqian Tang[3],Shiguang Miao[1]

1. Institute of Urban Meteorology, China Meteorological Administration, Beijing 100089, China

2. Environmental Meteorology Forecast Center of Beijing-Tianjin-Hebei, Beijing 100089, China

3. State Key Laboratory of Atmospheric Boundary Layer Physics and Atmospheric Chemistry, Institute of Atmospheric Physics, Chinese Academy of Sciences, Beijing 102300, China

Correspondence to: Xiujuan Zhao(xjzhao@ium.cn)

Abstract. Different types of pollution boundary layer structures form via the coupling of different synoptic systems and local mesoscale circulation in the boundary layer; this coupling contributes toward the formation and continuation of haze pollution. In this study, we objectively classify the 32 heavy haze pollution events using integrated meteorological and environmental data and ERA-Interim analysis data based on the rotated empirical orthogonal function method. The thermodynamic and dynamic structures of the boundary layer for different pollution weather types are synthesized, and the corresponding three-dimensional boundary layer conceptual models for haze pollution are constructed. The results show that four weather types mainly influence haze pollution events in the Beijing area: (a) type1: southerly transport, (b) type2: easterly convergence, (c) type3: sinking compression, and (d) type4: local accumulation. The explained variance in the four pollution weather types are 43.69% (type1), 33.68% (type2), 16.51% (type3), and 3.92% (type4). In persistent haze pollution events, type1 and type2 surpass 80% on the first and second days, while the other types are present alternately in later stages. The atmospheric structures of type1, type2, and type3 have typical baroclinic characteristics at mid-high latitudes, indicating that the accumulation and transport of pollutants in the boundary layer is affected by coupled structures in synoptic-scale systems and local circulation. The atmospheric structure of type4 has typical barotropic characteristics, indicating that the accumulation and transport of pollutants is primarily affected by local circulation. In type1, southerly winds with a specific thickness and intensity prevail in the boundary layer, which is favorable for the accumulation of pollutants in plain areas along the Yan and Taihang Mountains, whereas haze pollution levels in other areas are relatively low. Due to the interaction between weak easterly winds and the western mountains, pollutants accumulate mainly in the plain areas along the Taihang Mountains in type2. The atmospheric vertical structure is not conducive to upward pollutant diffusion. In type3, the heights of the inversion and boundary layers are the lowest due to a weak sinking motion while relative humidity is the highest among the four types. The atmosphere has a small capacity for pollutant dispersion and is

favorable to particulate matter hygroscopic growth; as a result, the type3 has highest $PM_{2.5}$ concentration. In type4, the boundary layer is the highest among the four types, the relative humidity is the lowest, and the $PM_{2.5}$ concentration is relatively lower under the influence of local mountain–plain winds. Different weather types will shape significantly different structures of the pollution boundary layer. The findings of this study allow us to understand the inherent difference among heavy pollution boundary layers; in addition, they reveal the formation mechanism of haze pollution from an integrated synoptic scale and boundary layer structure perspective. We also provide scientific support for the scientific reduction of emissions and air quality prediction in the Beijing-Tianjin-Hebei region of China.

1 Introduction

Over the past 40 years, rapid industrialization and urbanization have caused serious haze pollution problems in China,especially in the North China Plain (NCP). Beijing, located in the NCP region, suffers from frequent haze pollution, which has become one of the greatest issues of concern for the public and government (Huang, et al., 2018). High concentrations of fine particulates not only affect the climate system but also reduce visibility, affect city operation(Wang et al., 2015;Luan et al., 2018;Li et al., 2020), and have a significant negative impact on human health(Gong et al.,2019;Han et al.,2019,2020a,2020b,2020c). Haze pollution creates health costs for residents (Dockery et al., 1993; McDonnell et al., 2000) and emissions reductions costs (Hou et al., 2016).Governments must play a more flexible role and adopt an optimized strategy between health costs and economic costs of controlling emissions based on national or local economic affordability to reduce emissions (Lee et al., 2016).From an operability perspective, the timings of different emissions reductions strategies are largely dependent on trends in atmospheric pollution dispersion conditions (Zhai et al., 2016). Haze pollution is the combined effect that excessive emissions and adverse meteorological conditions have on the dispersion of pollutants (He et al., 2013; Li et al., 2017). With relatively few changes in the emission source, the diffusion conditions largely determine the duration and pollution level of a haze event.

First, from an atmospheric circulation perspective, persistent haze pollution generally corresponds to persistent adverse meteorological conditions for pollutant dispersion (Zheng et al., 2015), where persistent anomalies in atmospheric circulation are an important contributing factor (Inness et al., 2015).These conditions cause stabilized vertical stratification and low horizontal wind speeds (Chamorro et al., 2010; Park et al., 2014), such that the combination of these two conditions form "calm weather." From a large-scale climate circulation perspective (Markakis et al., 2017; Zou et al., 2017),previous studies have suggested that, if global warming trends continue, the probability of adverse atmospheric pollutant dispersion will continue to increase (Cai et al.,2017). The reduction in sea ice can lead to the weakening of the rossby wave activity south of 40°N, rendering the lower layer colder and a reduced moisture content, a stable atmosphere, weaker wind speeds, and an increased chance of heavy haze pollution(Wang et al.,2015;Chen et al.,2015).These results show that the troposphere in the Beijing-Tianjin-Hebei area can produce a continuous deep downdraft under flat circulation or a weak high-pressure system, along with the boundary layer's southerly wind yielding the temperature inversion height and decrease in the

atmospheric capacity, which provides a favorable dynamic condition for the maintenance and aggravation of haze pollution (Wu et al., 2017). Zhang et al. (2016) used the Kirchhofer technique (El-Kadi et al.,1992) to classify the circulation patterns during the time period of 1980-2013, examining the air quality associated with those patterns clarify. The circulation patterns were classified into 5 categories. The stagnant weather condition when wide-spread stable conditions controlled most part of NCP resulted in the highest air pollution. The westerly and southerly wind caused both the regional transport and local build-up of air pollutants.

Second, the pollutant concentration also depends on local mesoscale circulation coupled with a stable boundary layer and synoptic-scale system (Miao et al., 2017), for example, valley wind, sea–land wind, heat island circulation, and mountain–plain wind. Even under conditions associated with weaker synoptic circulations, these mesoscale systems largely determine the peak concentration and spatial-temporal distribution of the pollutants (Miao et al., 2017; Li et al., 2019). Millan et al.(1997), studied the mechanism of aerosol transport back and forth along the coast under the combined action of weather system, sea-land winds and slope wind.In coastal cities of West Africa,Adrien et al. (2019) simulated the transport and mixing processes of biomass combustion aerosols in the boundary layer and at the top of the boundary layer under the action of dry convection and sea breeze front. Tobias et al. (2017) studied pollution in coastal valley cities (Bergen, Norway), where the concentration of pollutants is determined by both large-scale topography and small-scale sea-land winds, when there is a strong background wind, the sea-land wind will submerge in the large-scale circulation, and the large-scale circulation and the local circulation in the boundary layer will cancel each other, causing ground-level air to stagnate and pollution levels to rise. Zhai et al.(2019) suggested that the easterly wind reached the strength of low-level jet streams and blew towards mountain in Beijing. Aerosols below 2.0 km were lifted to the upper atmosphere and blown downstream by the strong south-westerly wind. Quan et al. (2020) suggested that a combination of topography and planetary boundary layer (PBL) processes can drive the regional atmospheric pollutant transport over NCP. A mountain-induced vertical vortex elevated ground pollutants to form an elevated pollutant layer (EPL) which was transported to Beijing by southerly winds and downward to the surface through PBL processes finally.

In summary, meteorological conditions can be divided into a large scale circulation type and local meteorological conditions at different spatial scales. The circulation type governs local meteorological conditions and is effective in the identification of haze pollution. Although, many studies have investigated the influence of the circulation type on the haze pollution (or air quality) (Oanh et al., 2005; Zhang et al., 2016; Wu et al., 2017; He, et al., 2018). A comprehensive analysis combining weather systems and the structure of the boundary layer with objective synoptic classification method, however, is still rare. Liao et al. (2018) use the Self-Organizing Map method to classify the boundary layer in the Beijing area with radiosonde data. A continuum of nine atmospheric boundary layer types was obtained from the near neutral to strong stable conditions, which resulted in the dramatically increased of pollutants during all seasons except summer. For typical wintertime months, they suggested that atmospheric boundary layer types are one of the primary drivers of day-to-day $PM_{2.5}$ variations in Beijing. . Miao et al. (2017) use the obliquely rotated principal component analysis in T-mode (T-PCA) approach to classify

summertime synoptic patterns over Beijing. Three types of synoptic patterns (67% of the total) favoring the occurrence of heavy aerosol pollution were identified, which were characterized by southerly winds that favor the transport of pollutants to Beijing. The clouds and cold/warm advection modulate the planetary boundary layer structure in Beijing in the afternoon. Xu et al. (2019) also used T-PCA method to classify synoptic weather types during autumn and winter months in Shanghai. Their study indicated that transport resulted from cold front had significant impact on $PM_{2.5}$ levels in Shanghai, whereas persistent server pollution events were more closely related to weak pressure before high. All these studies presented a good view of air pollution formation influenced by weather system and planetary boundary layer structure with objective synoptic classification method. But the classifications of weather system or boundary layer meteorology were carried out separately, and the influences of these weather type or PBL type on air pollution were investigated for a long time average state. Classification of haze pollution weather types accompanying with different PBL structure and their associations with haze formation have seldom been reported in previous works, especially rare for the sever haze pollution events.

The Beijing area is located in the transition zone between the plain and mountainous areas, with mountains to the west, north, and east. The southeastern region of Beijing is a flat plain that slopes toward the Bohai Sea. More than 20 million people live in Beijing who are affected by both the weather system and local circulation in the boundary layer. To formulate optimized emissions reduction strategies, we must master the main control factors that affect the haze pollution diffusion conditions in Beijing under different weather and boundary layer conditions. In this study, based on the objective classification of persistent pollution weather types, we examine the boundary layer structures of different weather types, revealing that the thermal and dynamic mechanisms of the boundary layer structures influence the evolution of haze pollution. This study will extend previous studies as it is an attempt to investigate the meteorological mechanism of haze pollution formation from the perspective of interaction between weather system and boundary layer structure. In this paper, Sect. 2 provides descriptions of methodology and data. In Sect. 3, the pollution weather types are classified, and 3-D conceptual model for the pollution boundary layer is established for different weather types, and then their influences on spatial-temporal evolution of haze pollution are investigated. The main findings are summarized in Sect. 4.

2 Data and methods

2.1 Meteorological data

The weather classification data were derived from the ERA-Interim data from 2014–2017. ERA-Interim (0.125°×0.125°) is a new reanalysis data from the ECMWF (European Centre for Medium-Range Weather Forecasts) after the ERA40, with 60 vertical layers and partially overlaps with the ERA40 in time. However, significant progress has been made in data processing, for example, from the three-dimensional assimilation system(3-D VAR) to the four-dimensional assimilation system(4-D VAR). There are 4 soil moisture layers with the depth of 7cm, 28cm, 100cm and 255cm respectively. The model

128 contains 20 vegetation types, and the land surface parameters change with the change of vegetation types

129 (https://apps.ecmwf.int/datasets/).

130 The 850hPa geopotential height field (30–50°N, 110–128°E) of the ERA-Interim was used to classify the weather system.

131 The meteorological elements at 850hPa interact with the meteorological elements in the boundary layer. At the same time,

132 the 850hPa is evidently influenced by the free atmosphere, especially in Beijing area, which can be regarded as the transition

133 layer between local thermal circulation (valley wind, sea–land wind, and mountain–plain wind) and the free atmosphere. In

134 addition, the hourly relative humidity, visibility, and wind speed observed at the Beijing Observatory (39.93°N, 116.28°E)

135 were used in this study.

136 A 12-channel (5water channels and 7oxygen channels) microwave radiometer (Radiometrics, Romeoville, IL, U.S.A.) was

137 used to measure the hourly relative humidity and temperature profile in the atmosphere. The microwave radiometer was

138 installed in the Beijing Observatory (39.93°N, 116.28°E) and was calibrated every three months. The wind profiles,

139 including the wind speed and direction between 100 and 5,000m, are measured at the same station by a wind profiler. The

140 wind profiler radar provides a set of profile data every 6min at a detection height of ~12–16km, and hourly data were used in

141 this study. In data analysis, Beijing Local Time (BJT) was used.

142 **2.2 Air quality monitoring data and haze pollution event definition**

143 Hourly $PM_{2.5}$ concentrations at 12 national stations and the daily air quality index (AQI) in Beijing are available from

144 http://zx.bjmemc.com.cn/?timestamp=1564483254009. Surface $PM_{2.5}$ mass concentrations were measured by the tapered

145 element oscillating microbalance method. The measurements were calibrated and quality controlled according to the Chinese

146 environmental protection standard (HJ 618-2011).

147 As this study focuses on episodes of heavy haze pollution, we first defined the criteria. Haze is defined by the relative

148 humidity and visibility. Considering that haze pollution mainly refers to reduced visibility caused by fine particulate matter,

149 as well as taking into account the effects of the pollution levels and duration, the screening criteria for heavy haze pollution

150 were still based on the AQI, $PM_{2.5}$ concentration, and the duration of low visibility. The specific criteria of a haze pollution

151 event can be defined as follows: the AQI reaches a moderate pollution level (AQI≥150) for more than or equal to 3 days in

152 which at least 1 day reaches the heavy pollution level (AQI>200). The primary pollutant is $PM_{2.5}$ in Beijing area. As defined

153 by the AQI, the 24-h average concentration of $PM_{2.5}$must be above 115 μg m^{-3} for more than three consecutive days and

154 above 150 μg m^{-3} for at least 1 day. At the same time, the accumulated time of horizontal visibility, that is, less than 5 km,

155 has a duration of at least 12 h each day at the Beijing Observatory station.

156 Based on these criteria, 32 events (125 days) were screened for heavy haze pollution in Beijing between 2014 and2016.

157 Eight events occurred in spring and summer while 24 events were concentrated in autumn and winter, 32 events accounting

158 for 75% of the events that occurred during the study period (2014–2016). We collected ground-based routine meteorological

159 observation data in North China, L-band radar second-order sounding data (including wind, temperature, and humidity),

160 wind profile data, ceilometer data, and tower data during these events.

161 2.3 Attenuated backscattering coefficient measurements and boundary layer height calculation

162 2.3.1 Attenuated backscattering coefficient measurements

163 We used the CL31 and CL51 Vaisala-enhanced single-lens ceilometer instrument, which uses the pulse diode laser LIDAR

164 (laser detection and ranging) technology to measure the backscattering profile of atmospheric particles and the cloud height.

165 The main parameters of the CL31 and CL51 are respectively as follows: range of 7.6 and 13 km, reporting periods of 2–120

166 and 6–120s, reporting accuracy of 5and 10m/33ft, peak power of 310w, and wavelength of 910mm. The geographic location

167 of the station is 39.974°N and 116.372°E, with an elevation of approximately 60 m (Tang et al.,2016).

168 2.3.2 Boundary layer height calculation

169 As the lifetime of fine particles is long, that is, several days or weeks, the particles concentration in the boundary layer is

170 generally uniform, but is significantly different from that in the free atmosphere where particles concentration is much lower

171 (Lin et al.,2007;Kang et al.,2019). By analyzing the backscattering profile of the atmospheric particles, we located the abrupt

172 change in backscattering at the top of the boundary layer.

173 This study used the gradient method (Christoph et al., 2007; Zhang et al., 2013; Tang et al., 2015) to determine the boundary

174 layer heights. The maximum negative gradient in the aerosol backscattering coefficient profile occurs at the top of the

175 boundary layer, but is easily disturbed by data noise and the aerosol structure. Therefore, we must select a continuous region

176 of time or space for averaging to smooth the contour map vertically after averaging and adopt an improved gradient

177 (http://isars2010.uvsq.fr/images/stories/posterexabstracts/p_bls06_muenkel.pdf) method to manage severe weather (such as

178 precipitation and fog). Despite this, the gradient method still has certain defects, especially for neutral atmospheric

179 stratification, where the inverse calculation of the boundary layer height is not accurate.

180 2.4 Objective classification of pollution weather types

181 The 925 hPa geopotential height field is affected by both synoptic and local circulations, which can simultaneously reflect

182 the variation characteristics of weather system and boundary layer. Thus, the 925hPa geopotential heights of all pollution

183 events were analyzedin this study by using the 6h ERA-Interim reanalysis data. With 500 samples (4 times each day in 125

184 days), the rotated empirical orthogonal function (REOF) was used to determine which mode the pollution events belong to

185 according to the characteristic values of the different pollution events. (Paegle et al.,2002;Li et al.,2009). Since Lorenz (1956)

186 introduced empirical orthogonal function (EOF) analysis to atmospheric science, this simple and effective method has been

187 widely used in atmospheric, oceanic and climatic studies. The essence of EOF analysis is to identify and extract the

188 spatiotemporal modes that are ordered in terms of their representations of data variance(Lian et al.,2012). In the empirical

189 orthogonal function (EOF) analysis, the first few main components are the focus of the analysis element variance, such that

190 the EOF method can highlight the entire correlation structure of the analysis element. However, the local correlation

191 structure is not sufficient, which is a defect of the pollution weather classification based on the EOF. The spatial patterns

192 (EOFs) and the temporal coefficients of these modes are orthogonal. This orthogonality has the advantage of separating
193 unrelated patterns, but it sometimes leads to the complexity of spatial structure and the difficulty of physical interpretation
194 (Hannachi, 2007). Based on the EOF analysis, the REOF transforms the load characteristic vector field into a maximum
195 rotation variance, as a result of which each point in the rotation space vector field is only highly correlated with one or a few
196 rotation time coefficients. Previous studies have shown that REOF analysis can avoid non-physical dipolelike EOF analysis
197 patterns, which often occur when known dominant patterns have the same symbols in the region (Dommenget et al.,2002).
198 REOF analysis outperforms EOF analysis almost certainly in reconstructing spatially overlapped modes, and that this
199 superiority is not sensitive to parameters such as the number of modes, the spatial scale of the signal, and the degree of
200 rotation(Lian et al.,2012). Thus, the high load value areas are concentrated in smaller areas, while the remaining areas are
201 relatively small and nearly 0, highlighting the pattern and characteristics of the abnormal distribution of elements (Paegle et
202 al., 2002; Chen et al., 2003), the classification of heavy pollution weather types based on this method is more consistent with
203 the requirements of this study. Pollution weather types were classified by the REOF method to analyze the differences in the
204 structures of the pollution boundary layer.

205 **3Results and discussion**

206 **3.1 Pollution weather type classification and horizontal characteristic analysis**

207 In this study, the 925hPa geopotential height was used to classify the pollution weather types into four categories with the
208 REOF method, as shown in Fig. 1: (a) type1, that is, influenced by southerly winds at the rear of the high pressure system, (b)
209 type2, that is, influenced by easterly winds at the bottom of the high pressure system, (c) type3, that is, a weak downdraft
210 effect in the high pressure system, and (d) type4: no significant weather system. In this study, we observed 125 days of
211 heavy polluted weather. Among these days, type1, type2, type3, and type4 had 67, 27, 21, and 10 days, respectively (Fig.2),
212 where the four weather types accounted for 53.6, 21.6, 16.8, and 8.0% of the total sampled weather event days, respectively.
213 The total interpretation variance of the four types for all events was 97.8% while the independent interpretation variance was
214 43.69, 33.68, 16.51, and 3.92%, respectively (Fig. 2). This indicates that an objective weather classification can effectively
215 obtain the main feature information of the pollution weather types.
216 As shown in Fig. 1, the Beijing area is located toward west of the high-pressure system that has its center located in the sea.
217 The low pressure system is located in the northern Hebei province for type1, where southerly winds control the 925hPa,
218 which is favorable for the regional transportation of pollutants. Type1 is similar to the results of pattern2 and pattern4 by
219 Zhang et al. (2016) accompanied by regional transmission characteristics. Type1 is also similar to the results of type 1 by
220 Miao et al. (2017) with southerly winds throughout the layer. When type2 appears, the Beijing area is located at the bottom
221 of the high pressure system in Northeast or North China. In the plain area, the sea level pressure in the eastern part of Beijing
222 is higher than that in the central Beijing area, such that there is an evident pressure gradient. Due to pressure-gradient forcing,
223 the boundary layer appears within the easterly wind component while the easterly wind speed is smaller, which leads to

224 pollutant convergence into the plains along the Taihang Mountains, When type3 appears, the high pressure center is located
225 in the middle of Mongolia, where Beijing is in the front of the weak high pressure system, with a northwest current at
226 925hPa. However, the wind speed is lower than that affected by strong cold air, because of which it is difficult to penetrate
227 the lower layer of the boundary layer and the wind can only exist in the upper atmosphere of the boundary layer. When type4
228 appears, western Mongolia is a high pressure region and Southern Hebei province is a low pressure area, where there is only
229 a low pressure system with a smaller spatial and temporal scale. The synoptic-scale low pressure system is already located
230 over the sea in the eastern Jianghuai region, showing that the high and low pressures corresponding to the synoptic-scale
231 system are far from the Beijing area, which results in a weak synoptic-scale pressure gradient in Beijing and the surrounding
232 areas (Fig. 1d). Most areas in North China do not have strong weather systems and the average wind speed in the boundary
233 layer is smaller, which is favorable to the formation and maintenance of the local circulation considering the topography in
234 the Beijing area (Fig. 1i). The wind speed of type4 in the lower boundary layer is more difficult to regulate via the evolution
235 of the wind field based on the effect of descending momentum. Therefore, the dynamic pollutant process in the boundary
236 layer in type4 is more related to the local circulation.

237 **3.2 Vertical thermal and dynamic structure characteristics under four weather types**

238 The vertical structure of the atmosphere is very important for the formation and evolution of extreme haze events. The
239 vertical thermal and dynamic structures of four weather types are investigated in three-dimensional view. Figure 3 to Figure
240 6 presented the vertical distribution of temperature, wind and RH, respectively. The temperature in Fig. 3 and vertical speed
241 profiles in Fig.5 are averaged for each weather type by using the 6h ERA-Interim reanalysis data, respectively. The hourly
242 mean wind profiles in Fig.4 are observed at the Beijing Observatory, and the hourly mean relative humidity in Fig.6 is
243 measured with a microwave radiometer at the same site. According to the classification of weather type, the spatial-temporal
244 average analysis of the observed data is carried out. To classify the pollutant regimes according to the various meteorological
245 features, we summarized relevant thermodynamic and dynamic parameters in Table S1.
246 Figure 3 shows that the strong inversion is located at 800–900hPa for type1. In type2, easterly winds with low temperatures
247 influence the temperatures below 800hPa, where a cooling layer appears at 900 hPa, with the height of inversion between
248 700 and 800hPa. The inversion height for type3 is the lowest among the four types due to the sinking motion, where the
249 inversion is mainly below 900hPa, which causes a rapid decline in the atmospheric capacity. The atmospheric structure is
250 also relatively stable in type4, whose inversion structure is similar to type2. However, the inversion intensity (0.4°C) in type4
251 are weaker than that in type2 (0.7°C), and the wind speed is also small in type4.
252 As shown in Fig. 4, the basic flow is the southerly wind below 2,000m in type1, where a southwest wind appears from 500–
253 2,000m. The south wind is below 500m between 04:00 BJT and 20:00 BJT, and the easterly wind appears at other times. The
254 south wind speed below 500m is 4-6 m s^{-1} which is higher than the easterly wind(2-4 m s^{-1}). In type2, the basic flow above
255 1,000m is westerly wind, where the layer between 500 and 1,000m is a weak wind layer. We note that the wind velocity in
256 this layer is the smallest when there is an increase in the easterly component below 500m.This indicates that the weak wind

257 layer is the wind shear transition layer between the westerly wind above 500m and the easterly wind below 500m. The
258 easterly and westerly winds cancel each other at this height and form a small wind velocity layer. From 04:00 BJT to 20:00
259 BJT, southerly winds appear below 500m while we observe the appearance of easterly winds at other times. The space-time
260 structure of the wind field below 500 m was similar to that of type1, but the southerly wind speed was lower than in case of
261 type1.In type3, the wind above 500m originates from the northwest from 04:00 BJT to 14:00 BJT. At altitudes below 500 m,
262 the wind is southerly during these hours and northerly at other times. Whether it is southerly or northerly, the wind speed is
263 smaller. Mountain–plain wind in the Beijing area causes this diurnal and nocturnal circulation of the wind field. In type3, the
264 wind velocity below 500m is less than that of type1 and type2, because the basic flow is northerly, where northerly wind
265 superposes onto the plain wind (southerly), which may weaken the southerly wind speed. The observed data are the
266 superposition results of two scale wind fields (i.e. local circulation and synoptic airflow). Westerly or weak northerly winds
267 above 1,000m in type4 control the atmosphere, where the wind velocity below 1,000m is significantly weak. For the
268 majority of the time, the wind velocity is less than 4 m s^{-1}, but the mountain–plain diurnal cycle wind can still be observed
269 from the diurnal variation in the wind direction. From 08:00 BJT to 18:00 BJT, the wind is southerly while mainly northerly
270 at night. Weak wind speeds last for a long period in the boundary layer of type4, because of which the local thermal and
271 dynamic conditions can become the main factors that affect the spatial-temporal distribution of haze pollutants in Beijing.
272 Figure 5 shows that, above 700hPa, type1, type2, and type4 are ascending movements. The maximum of the synoptic scale
273 ascending movement appears in 900–950hPa.With an increase in the height, the intensity of the ascending movement
274 gradually weakens, whereas in type3, below 750hPa can be characterized as a sinking movement. The intensity of the
275 sinking movement increases gradually with decreasing pressure, where the maximum of the sinking movement appears at
276 900–950hPa.The intensity of the subsidence movement from this layer at 900–950hPa to the ground decreases a second time.
277 Therefore, the sinking movement affects the inversion layer of type3, where the height of the inversion layer is the lowest of
278 all types, resulting in type3 characterized by the smallest atmospheric capacity among the four types.
279 Based on Figure 6, the relative humidity profiles for the four weather types have both similarities and differences in their
280 space-time structures. The similarities in the four types are the increased and decreased relative humidity below 1,000m
281 during the night and day, respectively, with a reverse in the relative humidity appearing at an altitude about 500 m during the
282 day. The relative humidity of the surface layer decreases daily from 10:00 BJT to 20:00 BJT with an increase in the solar
283 radiation. The thickness of the dry layer in the surface layer increases continuously, reaching its maximum height at ca.
284 14:00 BJT or 15:00 BJT every day, but the maximum height of the dry layer does not exceed 500m. The top of the dry layer
285 is the reverse of the relative humidity layer. Above 1,000m, the relative humidity of the other three types, except type2,
286 decreases significantly during the day. However, the relative humidity increased evidently in type4 above 2,000m. As
287 mentioned in section 3.1, in type4, Beijing is located between a high pressure and a low pressure and in the front of the weak
288 frontal zone. Stratus cloud with high stability is located in the front of the weak frontal zone above 2,000m, so relative
289 humidity above 2,000m is higher.

290 The difference in the relative humidity field among the four types can be summarized as follows. The average relative
291 humidity below 1,000m is higher than that above 1,000m. The inverse relative humidity structure appears below 500m in
292 type2 and type3 from 00:00 BJT to 05:00 BJT, with a maximum relative humidity center of more than 90%. Above 500m,
293 the relative humidity also increases from 05:00 BJT to 12:00 BJT. The relative humidity structures of type1, type2, and
294 type3 all contain a baroclinic structure from lower to higher levels, where the baroclinic structure in type2 is more evident
295 because the basic flow in type2 is westerly, which reflects the baroclinic characteristics of the atmosphere in the mid-high
296 latitudes of East Asia. The basic flow is generally westerly in this area, where type1 and type3 are more typical of the
297 disturbances in the northerly and southerly wind in the westerlies, which is the fluctuation feature of the basic flow (Fig. 6).
298 The relative humidity profile in the pollution boundary layer formed under the condition of wave-current interaction in the
299 atmosphere.

300 Type2 has strong westerly characteristics below 3,000m (Fig. 4), which reflects more baroclinic characteristics in the
301 atmospheric vertical structure for the westerlies. Based on the analysis of the wind field, type4 is characterized by an average
302 wind speed that is the weakest among the four types. Three important factors determine the baroclinicity, that is, the density
303 gradient, pressure gradient, intersection angle between the density surface and pressure surface. This may be an important
304 factor why relative humidity field has more barotropic characteristics. From the analysis of the baroclinic and barotropic
305 characteristics, we can observe that the weather systems of type1, type2, and type 3 have a significant influence on the
306 accumulation and transport of pollutants in the Beijing area. The mountain–plain wind in type4 can occur due to weakening
307 in the weather system (Fig. 4).

308 **3.3 Construction of 3-D conceptual model for the pollution boundary layer**

309 Based on the characteristics of the circulation field and the vertical thermodynamic structure for the four weather types, we
310 established conceptual models of the boundary layer structure under the influence of the four pollution weather types.
311 Because the vertical axes are different for the wind profile and temperature profile, we chose the pressure axis, which is
312 widely used in meteorology, to make conceptual model. In Beijing area, 700hPa,850hPa and 925hPa are generally located at
313 a height of about 3,000m,1,500m and 800m, The four types are: (a) type1: southerly transport; (b) type2: easterly
314 convergence; (c) type3: sinking compression; (d) type4: local accumulation (Fig. 7). When type 1 appears, the Beijing area is
315 located at the rear of the high-pressure system, consistent with southerly winds throughout the atmosphere (Fig.1e and Fig.4),
316 and multilayer inversion occurs in the boundary layer (Fig. 3). Under the influence of a southerly wind, haze pollutants
317 accumulate in front of the Yan and Taihang Mountains. The air pollutants in the Hebei region have evident regional transport
318 features (Fig. 1). When type2 appears, the Beijing area is located at the bottom of the high-pressure system, where the air
319 above 850hPa (about 1500m in Beijing) is a westerly wind, with easterly winds below 850hPa. Under the influence of
320 easterly winds below 850hPa, haze pollutants tend to accumulate in front of the Taihang Mountains. The cross-mountain air
321 mass flows from west to east, preventing the further dispersion of air pollutants in front of the Taihang Mountains. When
322 type3 appears, a weak high-pressure system controls the Beijing area. A weak subsidence northwest flow influences the

atmosphere above 850hPa, which further compresses the capacity of the atmosphere to absorb pollutants in the boundary layer. The southerly wind at 850hPa is favorable for pollutant transportation in the region and accumulation in front of the Yan and Taihang Mountains. The atmospheric vertical structure in the high-level northwest wind and low-level southward wind provides excellent conditions for the stability of atmospheric stratification with respect to dynamic conditions and a thermal structure. The 850hPa southerly winds favor regional pollutant transport and their accumulation in the area along the Yan and Taihang Mountains. The atmospheric vertical structure of the high-level northwest wind and low-level southerly wind provides excellent conditions for stratification stability in terms of dynamic-thermal structures because southerly wind at 850hPa is warm advection, where advection inversion can form in the boundary layer, while weak subsidence above 850hPa can cause subsidence inversion. These two inversion mechanisms are coupled at the interface between the northwest wind and southerly wind, resulting in stable atmospheric stratification. When type4 appears, there is often no evident synoptic-scale system surrounding Beijing, with a weak pressure gradient above 850hPa. Therefore, the average wind speed is weak. The most important local circulation in Beijing, that is, the mountain–plain wind, begins to form in the boundary layer and plays an important role in the spatial and temporal distribution of atmospheric pollutants, with the wind direction continuously shifting from the south to the north. The air pollutants accumulate near the terrain convergence line formed by the mountain–plain wind. The terrain convergence line also swings from north to south, such that air pollution in the Beijing area often appears as a "different sky" relative to a clean sky in the north and a polluted sky in the south.

3.4 Effects of the four pollution weather types

3.4.1 Statistical analysis: effects of the four weather types on haze pollution

Figure 8 shows the statistical characteristics of the $PM_{2.5}$ concentrations and meteorological elements in terms of the four polluted weather types. The daily average $PM_{2.5}$ concentration in type3 is the highest at 245 μg m^{-3} and type4 is the lowest at 181μg m^{-3} (Fig. 4). The daily average relative humidity values of the four pollution weather types are >60%, with a maximum relative humidity of 72.3% in type3 and a minimum relative humidity of 63.5% in type4 (Fig. 8b).Under the influence of a high relative humidity and high $PM_{2.5}$ concentration, the daily average visibility for the four heavy pollution weather types is less than 4,000m, with a minimum daily average visibility of 2,193m in type1. The maximum daily average visibility is 3,624m in type4 (Fig. 8c). The mean 24h wind speeds for the four pollution weather types are all less than 2.0 m s^{-1}.

The mean daily wind speeds of type1 and type3 are both smaller, that is, 1.38 and 1.49 m s^{-1}, respectively. The mean daily wind speeds of type2 and type4 are relatively higher, that is, 1.70 and 1.76 m s^{-1}, respectively (Fig. 8d). There is a significant negative correlation between the boundary layer height and $PM_{2.5}$ concentration. The lowest boundary layer height was 386.5 m for type3, followed by type1, whereas type4 had the highest boundary layer height.

In this study, we calculated the distribution of the weather types from the first to last day of the persistent haze pollution events (Fig. 9). The daily synoptic types from the first to eighth day of persistent haze pollution events were calculated. As

the number of pollution events that lasted more than five days is relatively small, the classification results were combined with the statistics for the events defined as greater than or equal to five days. The results show that the cumulative proportion of type1 and type2 occurrences on the first and second pollution day are more than 80%, indicating that regional transport plays a more prominent role in the initial stage of haze pollution formation, which is consistent with previous analyses (Zhong et al.,2018). On the third day and thereafter, the proportion of type1 began to decrease, but still exceeded 30%. Type2, type3, and type4 began to alternately affect the Beijing area. This indicates that, after the first and second days, the center of high pressure over East China in type1 began to move eastward away from the mainland. Beijing is located at the rear of the high-pressure system, where the $PM_{2.5}$ concentration corresponding to type1 increases throughout most of the day. The timing of the initial rise in the $PM_{2.5}$ concentration is the earliest among the four types (Fig. 10a), which indicates the role of the rear within the high-pressure system in the transmission of pollutants (Fig. 11). When the upstream weather system begins to affect the Beijing area, it is occasionally located at the bottom of the high-pressure system (type2). The diurnal variation in the $PM_{2.5}$ concentration in type2 was similar to the mean annual variation in the $PM_{2.5}$ concentration in the Beijing area. The first peak was at 10:00 and the second was at 20:00(Zhao et al., 2009) (Fig. 10a). Easterly or southeasterly winds appear near the ground and the concentration of $PM_{2.5}$ in Tianjin drops (Fig. 11).The weak high-pressure system in type3 can directly affect the haze pollution diffusion conditions in the Beijing area, but the intensity of the cold air behind the upper trough is weak. The $PM_{2.5}$ concentration in type3 is higher at night and lower during the day, with the highest average $PM_{2.5}$ concentration among the four types. Based on this analysis, we can observe that, in type3, the height of the inversion layer is the lowest and the atmospheric capacity to contain pollutants is also the lowest under the influence of a weak downdraft (Fig. 10a). This has resulted in very small wind speed near the ground and large areas of air pollution in the north of China(Fig. 11). In type4, there is no evident weather system that affects the Beijing area. An increase in the thermal difference between the mountain and plain affects local circulation development. A shear line of wind field formed by local circulation can be seen in the North China Plain (Fig. 11).The average $PM_{2.5}$ concentration in type4 is the lowest among the four types. The diurnal variation in the $PM_{2.5}$ concentration shows a typical "v" pattern. After sunrise, the $PM_{2.5}$ concentration begins to decrease while, after sunset, the $PM_{2.5}$ concentration increases significantly, which was due to the fluctuation of aerosols under local meteorological conditions (Fig. 10a). Based on Fig. 10b, the boundary layer height of type3 is the lowest among all types for most part of a day, which is mainly related to the suppression of the weak synoptic-scale downdraft. The change in the trend of the boundary layer height is similar between type 2 and type 4 for most of the day. However, the boundary layer height is less developed when the thermal conditions are strongest between 12:00 and 18:00, which is similar to type3. The boundary layer heights of type2 and type4 are relatively high, and the corresponding $PM_{2.5}$ concentrations are the lowest out of the four pollution types (Fig. 10b).

The above analysis shows that in one persistent multi-day pollution event, the weather patterns that affect the Beijing area change daily, that is, they also change according to the basic principles of synoptic dynamics, which is the natural development and evolution of rossby waves in the mid-high latitude westerly belt. This also indicates that it is not appropriate to classify a multi-day pollution event as a defined type (such as the low-pressure or high-pressure type). We

390 cannot rule out the possibility that a pollution event may occur for several consecutive days under the influence of a low-
391 pressure system, which is a rare event. Even then, this may also be a combination of different low-pressure systems. In
392 addition, we note that, in one persistent multi-day heavy pollution event, different types of pollution weather types are linked
393 together in a permutation that affects the structure of the boundary layer and thus the change in the $PM_{2.5}$ concentration (Fig.
394 9). As different types of weather systems form different haze pollution events, we discuss the type of boundary layer
395 structure formed by certain weather systems in the Beijing area and how this boundary layer structure influences the
396 evolution of haze pollution formation in the next section.

3.4.2 Effects of four weather types on the 3-D spatial-temporal evolution of haze pollution

398 An example of a five-day haze process (December 22 to 26,2015) is adopted to investigate the effects of four weather types
399 including the boundary layer structure on the three-dimensional structure of the haze pollution process. December 22 is
400 type1, the whole layer is southerly wind (Fig. 13) and the ground is the convergence zone(Fig. 12), which facilitates regional
401 pollutant transport (Fig. 14). The vertical wind speed is weak upward movement (Fig. 13)and the temperature inversion is
402 maintained throughout the day(Fig. 15), which is favorable for the accumulation of pollutants..Under the influence of
403 southerly winds, the sensitive source areas related to the Beijing area are generally the plain areas along the Taihang
404 Mountains in Hebei province (Wang et al., 2017). According to the dynamics, the positive vorticity advection in the
405 direction of Beijing forms in the plain area. The positive vorticity advection in this boundary layer has two functions. First,
406 the positive vorticity airflow is affected by the friction, coriolis effect, and pressure-gradient force. Second, the positive
407 vorticity advection continuously transports the converging space field to the Beijing area and, at the same time, also transfers
408 a large amount of external pollutants.

409 Type3 is on December 23. The ground is controlled by high pressure(Fig. 12), the atmosphere is prevailing northwest wind
410 below 3,000m(Fig. 13), and the boundary layer height further decreases(Fig. 15). There are few relevant studies on type3.
411 Because in the past, when the northerly wind appears, it indicates the arrival of cold air and the diffusion conditions will
412 improve, but sometimes this is not the case. We found that the research results of Wu et al.(2017) put emphasis on the
413 importance of subsidence motion on haze formation mechanism in the conceptual model, which is consistent with the key
414 role of weak subsidence motion in type3.The thickness of haze layer formed by regional transmission and local accumulation
415 is less than 300 m (Fig. 14).

416 Type4 is on December 24th, and the ground is the convergence zone (Fig. 12). The aerosol concentration and relative
417 humidity in Beijing area drops rapidly and then rises rapidly, and the boundary layer rises to more than 1500m during the
418 period when the aerosol concentration drops(Fig. 14 and Fig. 16). Under the action of weather system and local circulation,
419 the pollution zone in the boundary layer swings southward and northward. There are some research achievements on aerosol
420 of local circulation, which are generally carried out from the aspects of mountain topography and land-sea distribution with
421 local characteristics (Li et al.,2018; 2020). These studies require observations with high spatial and temporal resolution to
422 identify boundary layer structures.

Type3 occurs on December 25 once again, when the northwest wind appears again in the upper atmosphere, the vertical movement is a continuous weak sinking movement (Fig. 13) and the boundary layer height continues to maintain below 300m(Fig. 14). The temperature inversion is maintained throughout the day(Fig. 15). December 26 is type2. Beijing area is located at the bottom of high pressure(Fig. 12), and easterly winds prevail in the lower layer of the boundary layer(Fig. 13). The diffusion conditions of air pollution here can be divided into two stages. In the first stage, the easterly wind is below 1,000m, and the northerly wind is above 1,000m, so the aerosol can not spread to the upper atmosphere(Fig. 13). In the second stage, the high pressure continued to move eastward and lost its influence on the Beijing area. When the northerly wind over 1,000m changed to the westerly or southwesterly wind, the upper and lower atmosphere were connected, and the upward movement of m s^{-1} magnitude was stimulated in the boundary layer(Fig. 13), the haze process ends when the aerosol is lifted into the upper atmosphere(Fig. 14).

4 Conclusion

In this study, we objectively classified pollution weather events based on the REOF method using integrated observation data from meteorology and the environment, combined with the ERA-Interim reanalysis data(0.125°×0.125°).We then synthesized the thermodynamic and dynamic structures of the boundary layer under the different pollution weather types to construct the corresponding boundary layer conceptual models. The results show that four weather types mainly affect the pollution events in Beijing: (a) type1: southerly transport,(b) type2: easterly convergence,(c) type3: sinking compression, and (d) type4: local accumulation. The explained variance in the four pollution weather types were 43.69(type1), 33.68 (type2), 16.51(type3), and 3.92% (type4), respectively.

In persistent pollution events, the proportion of type1 and type2 occurrences were more than 80% on the first and second days, with subsequent alternations to the other types. The atmospheric structures of type1, type2, and type3 have typical baroclinic characteristics in the mid-high latitudes, indicating that synoptic-scale systems, together with local circulation, affect the accumulation and transport of pollutants in the boundary layer. On the other hand, the atmospheric structures of type4 have typical barotropic characteristics, which indicates that local circulation plays a major role in pollutant accumulation and transport. This is the first time that the baroclinic and barotropic characteristics of the atmosphere have been introduced into the discussion of pollution boundary layer.

Among the four types, southerly winds, with certain thicknesses and intensities, appeared in the boundary layer of type1, which was favorable for the transportation of pollutants to Beijing, accumulating more in areas along the Yan and Taihang Mountains. On the other hand, the pollution level in the central plain area of Hebei was relatively small. For type2, the pollutants mainly concentrated along the Taihang Mountains due to the influence of the interaction between weak easterly winds and topography. The vertical structure of the atmosphere was unfavorable for pollutants to ascend into the mountains. Type 3 had the lowest inversion height, boundary layer height, and the highest surface relative surface humidity, which are favorable for PM$_{2.5}$ hygroscopic growth. Correspondingly, type3 had the highest PM$_{2.5}$ concentration. Type4 had the highest

455 boundary layer height and lowest surface relative humidity among the four pollution types, whose $PM_{2.5}$ concentration was

456 relatively low when exposed to local mountain–plain winds. Pollutant accumulation is related to dynamic oscillation along

457 the convergence line of the mountain terrain. The results of this study allow us to understand the formation mechanism of

458 different heavy pollution boundary layers from synoptic scale and boundary layer perspectives, as well as to provide

459 scientific support for scientific emissions reduction and air quality prediction. The different heavy pollution weather types

460 and heavy pollution boundary layers not only reflect the interaction between the atmospheric mean flow and fluctuation, but

461 also reflect the process of heavy pollution weather types shaping the boundary layer. In addition, through the analysis of 1-4

462 types pollution processes(December 22 to 26,2015), we further illustrate the influence of different weather systems on the

463 shaping of the pollution boundary layer in the continuous pollution process.

464 Although we attempted to collect data on all types of atmospheric pollution boundary layer structures in the Beijing area,

465 there are still certain data samples that were not collected. These data can also explain the pollution characteristics associated

466 with the four heavy pollution boundary layers from other factors, such as $PM_{2.5}$ composition data. We also speculate that

467 there is feedback between aerosols and the boundary layer, which was not examined in this study. Although there have been

468 numerous studies on atmospheric pollutant transport, there are few studies on 3-Dpollutant transportation, which will be the

469 focus of our future investigations.

470

471 *Data availability*. All the data are available upon request via email: xjzhao@ium.cn.

472 *Competing interests*. The authors declare that they have no conflict of interest.

473 *Acknowledgements*. This study is supported by the National Natural Science Foundation of China (41305130), Beijing Major

474 Science and Technology Project (Z181100005418014), the Natural Science Foundation of Beijing Municipality (8161004)

475 and the National Natural Science Foundation of China (41975004).

476

477

478

479

480

481

482

483

484

References

Adrien, D., Laurent M., Cyrille F., Joel, B., Cyrielle, D., Volker, Dreiling., Andreas, F., Corinne, J., Norbert, K., Peter, K., Russ, L., Sylvain, M., Marlon, M., Federica, P., Bruno, P., Guillaume, S., and Solène, T.:Diurnal cycle of coastal anthropogenic pollutant transport over southern West Africa during the DACCIWA campaign. Atmos. Chem. Phys., 19, 473-497, https://doi.org/10.5194/acp-19-473-2019 ,2019.

Cai, W. J., Li, K., Liao, H., Wang, H. J., and Wu, L. X.: Weather conditions conducive to Beijing severe haze more frequent under climate change, Nat. Clim. Chang., 7, 257-262, http://doi.org/10.1038/nclimate3249, 2017.

Chamorro, L. P., and Porte-Agel, F.: Effects of thermal stability and incoming boundary-layer flow characteristics on wind-turbine wakes: a wind-tunnel study, Bound.-Layer Meteor., 136, 515-533, http://doi.org/10.1007/s10546-010-9512-1, 2010.

Chen, G. T.-J., Jiang, Z., and Wu, M.-C.: Spring heavy rain events in Taiwan during warm episodes and the associated large-scale conditions, Monthly Weather Review, 131, 1173-1188, 2003.

Chen, H. P., and Wang, H. J.: Haze days in North China and the associated atmospheric circulations based on daily visibility data from 1960 to 2012, J. Geophys. Res.-Atmos., 120, 5895-5909, http://doi.org/10.1002/2015jd023225, 2015.

Dockery, D. W., Pope, C. A., 3rd, Xu, X., Spengler, J. D., Ware, J. H., Fay, M. E., Ferris, B. G., Jr., and Speizer, F. E.: An association between air pollution and mortality in six U.S. cities, N. Engl. J. Med., 329, 1753-1759, http://doi.org/10.1056/nejm199312093292401, 1993.

Dommenget, D., and Latif, M.: A cautionary note on the interpretation of EOFs. J. Climate, 15, 216-225, https://doi.org/10.1175/1520-0442(2002)015<0216:ACNOTI>2.0.CO;2,2002.

El-Kadi, A.K.A., Smithson, P.A.: Atmospheric classifications and synoptic climatology, Prog. Phys. Geogr., 16, 432-455, https://doi.org/10.1177/030913339201600403,1992.

Gong, T.Y., Sun, Z.B., Zhang, X.L., Zhang, Y., Wang, S.G., Han, L., Zhao, D.L., Ding, D.P., Zheng, C.J.:Associations of black carbon and PM2.5 with daily cardiovascular mortalityin Beijing, China. Atmos. Environ., 214, 116876, https://doi.org/10.1016/j.atmosenv.2019.116876,2019.

Hannachi, A.: Pattern hunting in climate: A new method for finding trends in gridded climate data. Int. J. Climatol., 27, 1-15, https://doi.org/10.1002/joc.1375 ,2007.

Han, L., Sun, Z.B., He, J., Zhang, X.L., Hao, Y., Zhang, Y.: Does the early haze warning policy in Beijing reflect the associated health risks, even for slight haze? Atmos. Environ., 210, 110–119,https://doi.org/10.1016/j.atmosenv.2019.04.051, 2019.

Han, L., Sun, Z.B., He, J., Hao, Y., Tang, Q.L., Zhang, X.L., Zheng, C.J., Miao, S.G.:Seasonal variation in health impacts associated with visibility in Beijing, China, Sci. Total. Environ.,730, 139149, https://doi.org/10.1016/j.scitotenv.2020.139149,2020.

Han, L., Sun, Z.B., He, J., Zhang, B.H., Lv, M.Y., Zhang, X.L., Zheng, C.J.: Estimating the mortality burden attributable to

temperature andPM2.5 from the perspective of atmospheric flow. Environ. Res. Lett., 15, 124059, https://doi.org/10.1088/1748-9326/abc8b9,2020.

Han, L., Sun, Z.B. , Gong, T.Y., Zhang, X.L., He, J., Xing, Q., Li, Z.M., Wang, J., Ye, D.X., Miao, S.G.: Assessment of the short-term mortality effect of the national actionplan on air pollution in Beijing, China. Environ. Res. Lett., 15,034052, https://doi.org/10.1088/1748-9326/ab6f13,2020.

He, K. B., Yao, Z. L., and Zhang, Y. Z.: Characteristics of vehicle emissions in China based on portable emission measurement system, 19th Annual International Emission Inventory Conference "Emissions Inventories-Informing Emerging Issues", San Antonio, Texas, 2010.

He, J.J., Gong, S.L., Zhou, C.H., Lu, S.H., Wu, L., Chen, Y., Yu, Y., Zhao, S.P., Yu, L.J., Yin, C.M.: Analyses of winter circulation types and their impacts on haze pollution in Beijing, Atmos. Environ., 192, 94-103, https://doi.org/10.1016/j.atmosenv.2018.08.060, 2018.

Hou, Q., An, X.Q., Tao, Y., Sun Z.B.: Assessment of resident's exposure level and health economic costs of PM10 in Beijing from 2008 to 2012, Sci. Total. Environ.,563-564,557-565, http://dx.doi.org/10.1016/j.scitotenv.2016.03.215,2016.

Inness, A., Benedetti, A., Flemming, J., Huijnen, V., Kaiser, J. W., Parrington, M., and Remy, S.: The ENSO signal in atmospheric composition fields: emission-driven versus dynamically induced changes, Atmos. Chem. Phys., 15, 9083-9097, http://doi.org/10.5194/acp-15-9083-2015, 2015.

Kang, H.Q., Zhu, B., Gao, J.H.,He,Y.,Wang,H.W.,Su,J.F.,Pan,C.,Zhu,T.,Yu,B.:Potential impacts of cold frontal passage on air quality overtheYangtze River Delta, China. Atmos. Chem. Phys., 19, 3673–3685,http://doi.org/10.5194/acp-19-3673-2019,2019.

Lee, Y., Shindell, D. T., Faluvegi, G., and Pinder, R. W.: Potential impact of a US climate policy and air quality regulations on future air quality and climate change, Atmos. Chem. Phys., 16, 5323-5342, http://doi.org/10.5194/acp-16-5323-2016, 2016.

Li, J., Du, H. Y., Wang, Z. F., Sun, Y. L., Yang, W. Y., Li, J. J., Tang, X., and Fu, P. Q.: Rapid formation of a severe regional winter haze episode over a mega-city cluster on the North China Plain, Environ. Pollut., 223, 605-615, http://doi.org/10.1016/j.envpol.2017.01.063, 2017.

Luan, T., Guo, X., Guo, L., and Zhang, T.: Quantifying the relationship between PM2.5 concentration, visibility and planetary boundary layer height for long-lasting haze and fog–haze mixed events in Beijing, Atmos. Chem. Phys., 18, 203–225, https://doi.org/10.5194/acp-18-203-2018, 2018.

Li, J., Sun, Z.B., Donald, H. L., Zhou, M.Y., Dou, Y.J., Cheng, Z.G., Wang, Y.T., and Li, Q.C.:Atmos. Chem. Phys., 20,15793–15809, https://doi.org/10.5194/acp-20-15793-2020, 2020.

Li, J.B., Cook, E. R., D'arrigo,R., Chen, F. H., Gou, X. H.:Moisture variability across China and Mongolia: 1951-2005. Climate Dynamics, 32(7-8):1173-1186, http://doi.org/10.1007/s00382-008-0436-0,2009.

Li, Q. C., Li, J., Zheng, Z. F., Wang, Y. T., and Yu, M.: Influence of mountain valley breeze and sea land breeze in winter on distribution of air pollutants in Beijing-Tianjin-Hebei region, Environmental Science, 40, 513-524, http://doi.org/10.13227/j.hjkx.201803193, 2019.

Li, J., Sun, J.l., Zhou, M.Y., Cheng, Z.G., Li, Q.C.,Cao, X.Y., and Zhang, J.J.: Observational analyses of dramatic developments of a severe air pollution event in the Beijing area. Atmos. Chem. Phys., 18, 3919–3935, http://doi.org/10.5194/acp-18-3919-2018, 2018.

Li, J., Sun, Z.B., Donald H, L., Zhou, M.Y. , Dou, Y.J., Cheng, Z.G., Wang, Y.T., and Li, Q.C.: A foehn-induced haze front in Beijing: observations and implications. Atmos. Chem. Phys.,20, 15793–15809, https://doi.org/10.5194/acp-20-15793-2020,2020

Liao, Z. H., Sun, J. R., Yao, J. L., Liu, L., Li, H. W., Liu, J., Xie, J. L., Wu, D., and Fan, S. J.: Self-organized classification of boundary layer meteorology and associated characteristics of air quality in Beijing, Atmos. Chem. Phys., 18, 6771-6783, http://doi.org/10.5194/acp-18-6771-2018, 2018.

Lian, T., Chen, D.:An Evaluation of Rotated EOF Analysis and Its Application to Tropical Pacific SST Variability. J. Climate, 25(15):5361-5373, https://doi.org/10.1175/JCLI-D-11-00663,12012.

Lin, C.Y., Wang, Z., Chen, W.N., Chang, S.Y. :Long-range transport of Asian dust and air pollutants to Taiwan:observed evidence and model simulation, Atmos. Chem. Phys., 7, 423–434, http://doi.org/10.5194/acp-7-423-2007,2007.

Lorenz, E. N.: Empirical orthogonal functions and statistical weather prediction. Dept. of Meteorology, Massachusetts Institute ofTechnology, Statistical Forecasting Project Rep. 1, 49 pp,1956.

Markakis, K., Valari, M., Engardt, M., Lacressonniere, G., Vautard, R., and Andersson, C.: Mid-21st century air quality at the urban scale under the influence of changed climate and emissions - case studies for Paris and Stockholm, Atmos. Chem. Phys., 16, 1877-1894, http://doi.org/10.5194/acp-16-1877-2016, 2016.

McDonnell, W. F., Nishino-Ishikawa, N., Petersen, F. F., Chen, L. H., and Abbey, D. E.: Relationships of mortality with the fine and coarse fractions of long-term ambient PM_{10} concentrations in nonsmokers, J. Expo. Anal. Environ. Epidemiol., 10, 427-436, http://doi.org/10.1038/sj.jea.7500095, 2000.

Miao, Y. C., Guo, J. P., Liu, S. H., Liu, H., Li, Z. Q., Zhang, W. C., and Zhai, P. M.: Classification of summertime synoptic patterns in Beijing and their associations with boundary layer structure affecting aerosol pollution, Atmos. Chem. Phys., 17, 3097-3110, http://doi.org/10.5194/acp-17-3097-2017, 2017.

Millan, M. M., Salvador, R., Mantilla, E., and Kallos, G.: Photooxidantdynamics in the Mediterranean basin in summer: Results from European research projects, J. Geophys. Res., 102(D7), https://doi.org/10.1029/96JD03610 ,1997

Munkel, C., Eresmaa, N., Rasanen, J., and Karppinen, A.: Retrieval of mixing height and dust concentration with lidar ceilometer, Bound.-Layer Meteor., 124, 117-128, http://doi.org/10.1007/s10546-006-9103-3, 2007.

Oanh, N.T.K., Chutimon, P., Ekbordin, W., Supat, W.: Meteorological pattern classification and application for forecasting air pollution episode potential in a mountain-valley area, Atmos. Environ. 39, 1211–1225. https://doi.org/10.1016/j.atmosenv.2004.10.015, 2005.

Paegle, J. N., and Mo, K. C.: Linkages between summer rainfall variability over South America and sea surface temperature anomalies, J. Clim., 15, 1389-1407, https://doi.org/10.1175/1520-0442(2002)015<1389:LBSRVO>2.0.CO;2, 2002.

Park, J., Basu, S., and Manuel, L.: Large-eddy simulation of stable boundary layer turbulence and estimation of associated wind turbine loads, Wind Energy, 17, 359-384, http://doi.org/10.1002/we.1580, 2014.

Quan, J.N., Dou, Y.J., Zhao, X.J., Liu, Q., Sun, Z.B., Pan,Y.B., Jia, X.C., Cheng, Z.G., Ma, P. K., Su, J., Xin, J.Y., Liu, Y.G.. Regional atmospheric pollutant transport mechanisms over the North China Plain driven by topography and planetary boundary layer processes. Atmos. Environ., 221, 117098,1-9, https://doi.org/10.1016/j.atmosenv.2019.117098,2020.

Tang, G., Zhu, X., Hu, B., Xin, J., Wang, L., Munkel, C., Mao, G., and Wang, Y.: Impact of emission controls on air quality in Beijing during APEC 2014: lidar ceilometer observations, Atmos. Chem. Phys., 15, 12667-12680, http://doi.org/10.5194/acp-15-12667-2015, 2015.

Tang, G. Q., Zhang, J. Q., Zhu, X. W., Song, T., Munkel, C., Hu, B., Schafer, K., Liu, Z. R., Zhang, J. K., Wang, L. L., Xin, J. Y., Suppan, P., and Wang, Y. S.: Mixing layer height and its implications for air pollution over Beijing, China, Atmos. Chem. Phys., 16, 2459-2475, http://doi.org/10.5194/acp-16-2459-2016, 2016.

Tobias, W. G., Igor, E., Joachim, R.: Sensitivity of local air quality to the interplay between smalland large-scale circulations: a large-eddy simulation study. Atmos. Chem. Phys., 17, 7261-7276, https://doi.org/1680-7324/acp/2005-5-3389, 2017.

Wang, C., An, X., Zhai, S., Hou, Q., and Sun, Z.: Tracking sensitive source areas of different weather pollution types using GRAPES-CUACE adjoint model, Atmos. Environ., 175, 154-166, http://doi.org/10.1016/j.atmosenv.2017.11.041, 2018.

Wang, H., Chen, H., and Liu, J.: Arctic sea ice decline intensified haze pollution in Eastern China, Atmospheric and Oceanic Science Letters, 8, 1-9, http://doi.org/10.3878/AOSL20140081, 2015.

Wang, H., Peng, Y., Zhang, X. Y., Liu, H. L., Zhang, M., Che, H. Z., Cheng, Y. L., and Zheng, Y.: Contributions to the explosive growth of $PM_{2.5}$ mass due to aerosol-radiation feedback and decrease in turbulent diffusion during a red alert heavy haze in Beijing-Tianjin-Hebei, China, Atmos. Chem. Phys., 18, 17717-17733, http://doi.org/10.5194/acp-18-17717-2018, 2018.

Wang, Y. H., Liu, Z. R., Zhang, J. K., Hu, B., Ji, D. S., Yu, Y. C., and Wang, Y. S.: Aerosol physicochemical properties and implications for visibility during an intense haze episode during winter in Beijing, Atmos. Chem. Phys., 15, 3205–3215, https://doi.org/10.5194/acp-15-3205-2015, 2015.

Wu, P., Ding, Y. H., and Liu, Y. J.: Atmospheric circulation and dynamic mechanism for persistent haze events in the Beijing-Tianjin-Hebei region, Adv. Atmos. Sci., 34, 429-440, http://doi.org/10.1007/s00376-016-6158-z, 2017.

Xu, J. M., Chang, L. Y., Ma, J. H., Mao, Z. C., Chen, L., and Cao, Y.: Objective synoptic weather classification on $PM_{2.5}$ pollution during autumn and winter seasons in Shanghai, Acta Scientiae Circumstantiae, 36, 4303-4314, http://doi.org/10.13671/j.hjkxxb.2016.0224, 2016.

Zhai, L., Sun, Z.B., Li, Z.M., Yin, X.M., Xiong, Y.J., Wu, J., Li, E.J., and Kou, X.X. : Dynamic effects of topography on dust particles in the Beijing region of China, Atmos. Environ.,213,413-423, https://doi.org/10.1016/j.atmosenv.2019.06.029,2019.

618 Zhai, S. X., An, X. Q., Liu, Z., Sun, Z. B., and Hou, Q.: Model assessment of atmospheric pollution control schemes for
619   critical emission regions, Atmos. Environ., 124, 367-377, http://doi.org/10.1016/j.atmosenv.2015.08.093, 2016.

620 Zhang, W., Zhang, Y., Lv, Y., Li, K., and Li, Z.: Observation of atmospheric boundary layer height by ground-based LiDAR
621   during haze days, Journal of Remote Sensing, 17, 981-992, 2013.

622 Zhang, Y., Ding, A. J., Mao, H. T., Nie, W., Zhou, D. R., Liu, L. X., Huang, X., and Fu, C. B.: Impact of synoptic weather
623   patterns and inter-decadal climate variability on air quality in the North China Plain during 1980-2013, Atmos. Environ.,
624   124, 119-128, http://doi.org/10.1016/j.atmosenv.2015.05.063, 2016.

625 Zhao, X., Zhang, X., Xu, X., Xu, J., Meng, W., and Pu, W.: Seasonal and diurnal variations of ambient $PM_{2.5}$ concentration
626   in urban and rural environments in Beijing, Atmos. Environ., 43, 2893-2900,
627   http://doi.org/10.1016/j.atmosenv.2009.03.009, 2009.

628 Zheng, X. Y., Fu, Y. F., Yang, Y. J., and Liu, G. S.: Impact of atmospheric circulations on aerosol distributions in autumn
629   over eastern China: observational evidence, Atmos. Chem. Phys., 15, 12115-12138, http://doi.org/10.5194/acp-15-12115-
630   2015, 2015.

631 Zou, Y. F., Wang, Y. H., Zhang, Y. Z., and Koo, J. H.: Arctic sea ice, Eurasia snow, and extreme winter haze in China,
632   Science Advances, 3, http://doi.org/10.1126/sciadv.1602751, 2017.

633
634

635

Figures and figure captions
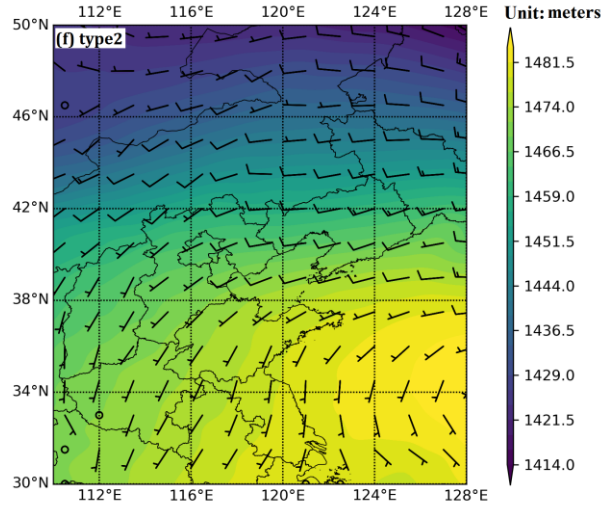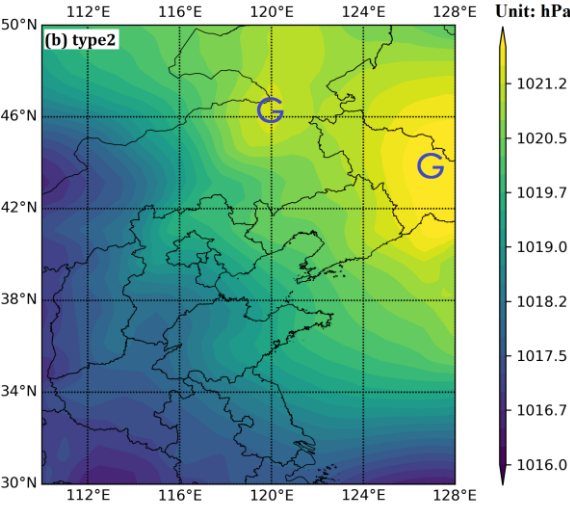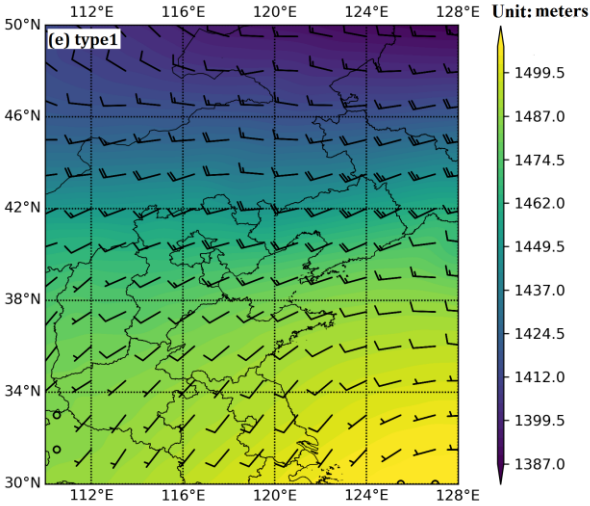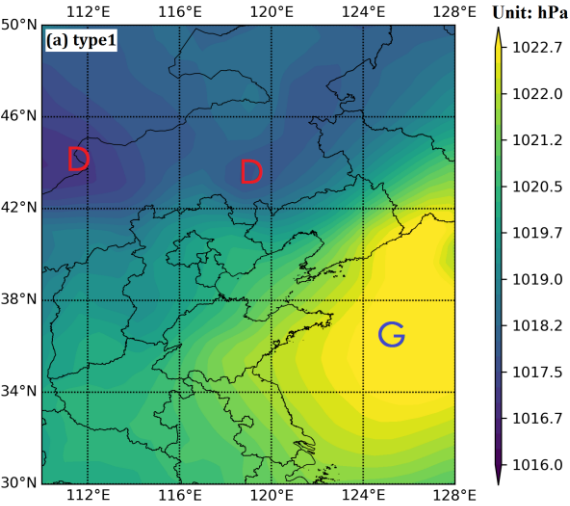
639
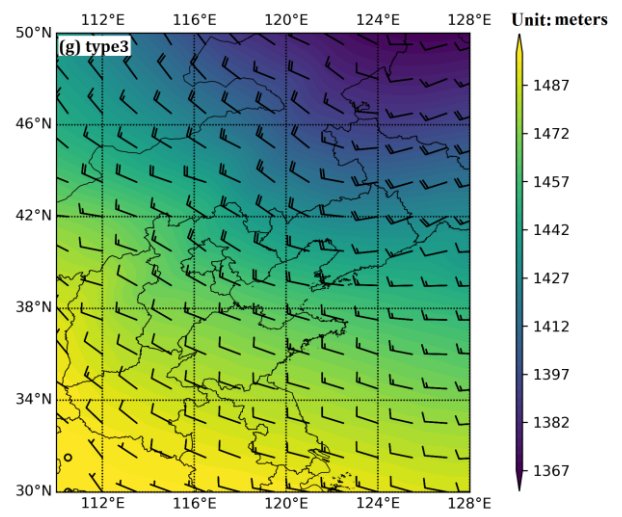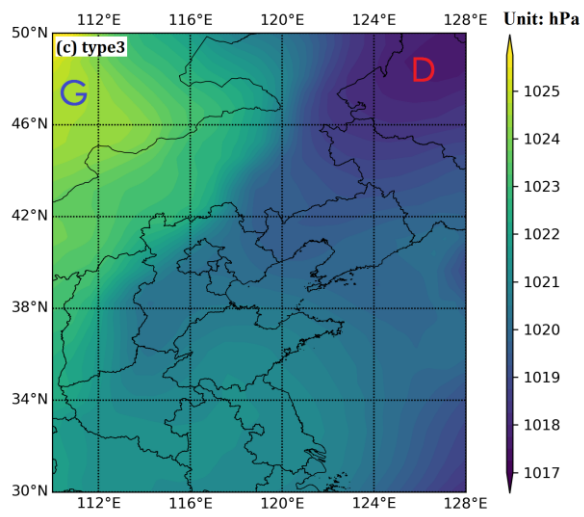
640
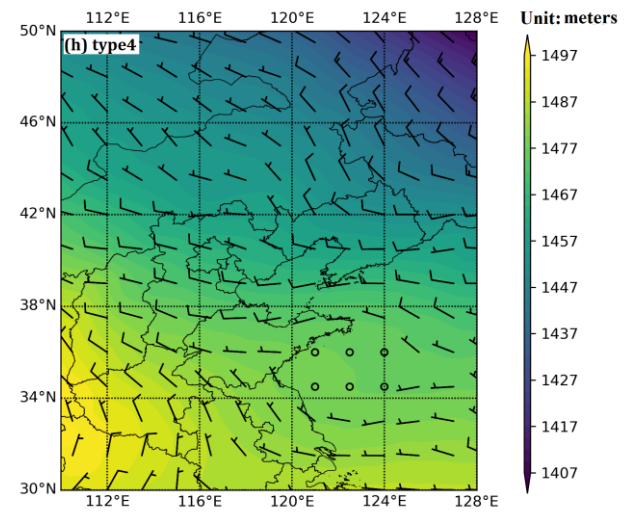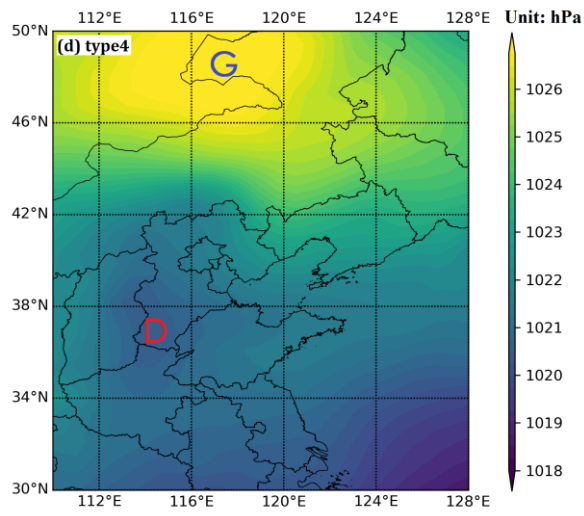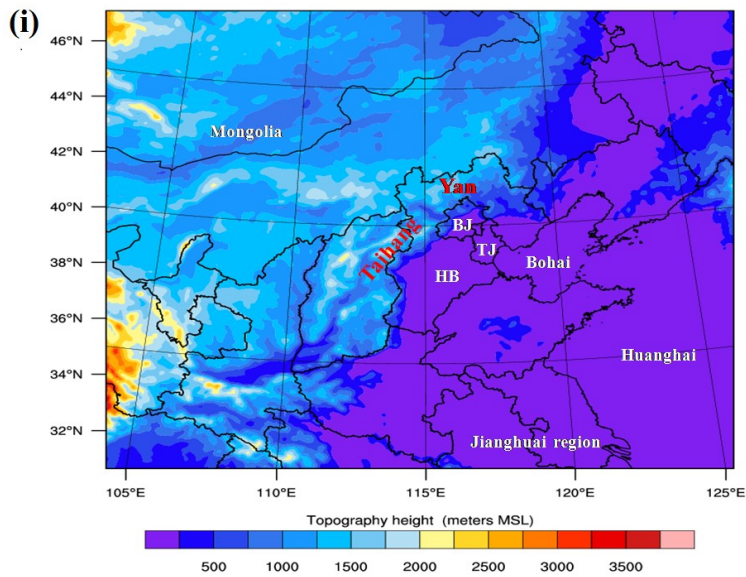
641

642 Figure 1. Sea level pressure (unit: hPa, top), geopotential height of 925hPa(unit: gpm, bottom), wind field (wind direction

643 bar)for the four heavy pollution weather types in the Beijing area: (a and e) type1, (b and f) type2, (c and g) type3, and (d

644 and h) type4. Topography height of the North China (i, unit:m). BJ,TJ and HB represent Beijing, Tianjin and Hebei. Yan and

645 Taihang represent Yan and Taihang montains.

646

647

648

649
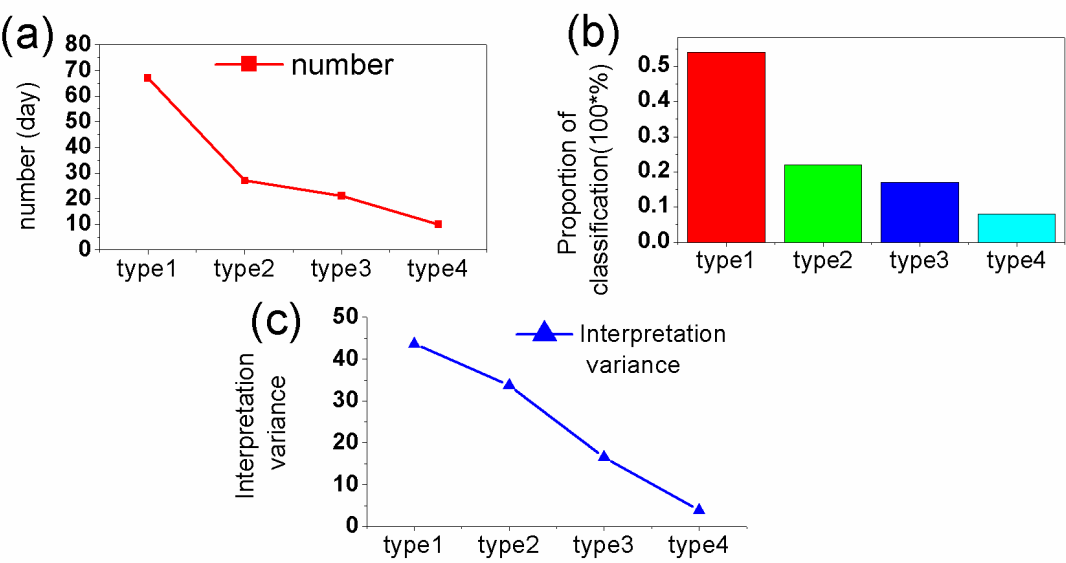
Figure 2.The four pollution weather types as a function of their (a) number of samples,(b) proportion with respect to the total

number of samples, and (c)interpretation variance.

652

653

654
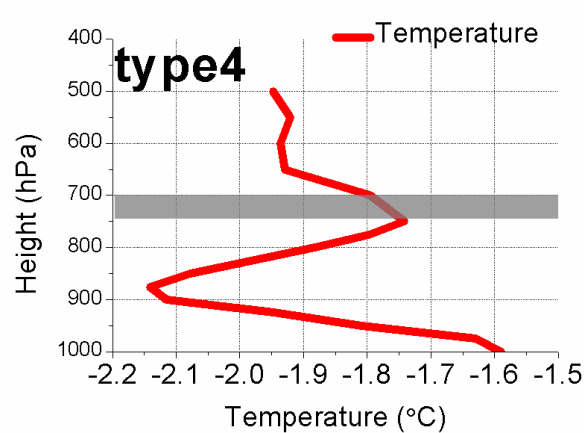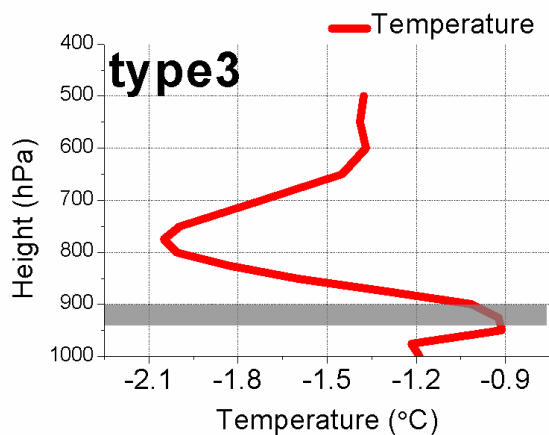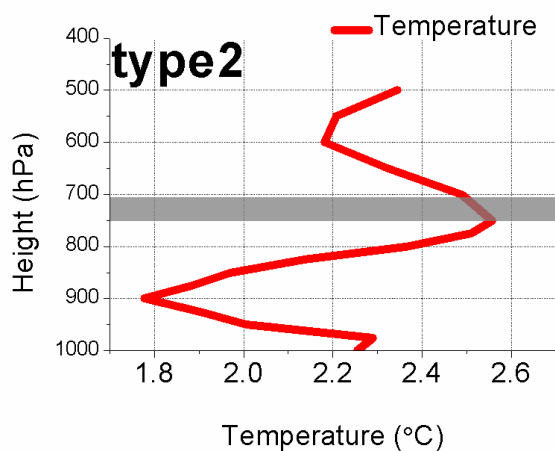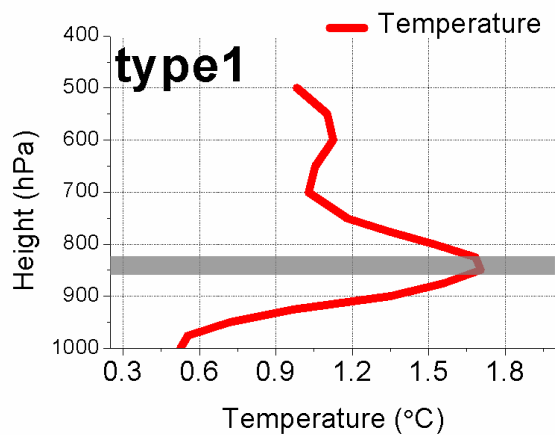
Figure. 3 Vertical distribution of temperature in pollution boundary layer of four types in Beijing area .Solid red lines
represent temperatures at different heights. Gray shade represents the top of the inversion layer.

657

658

659
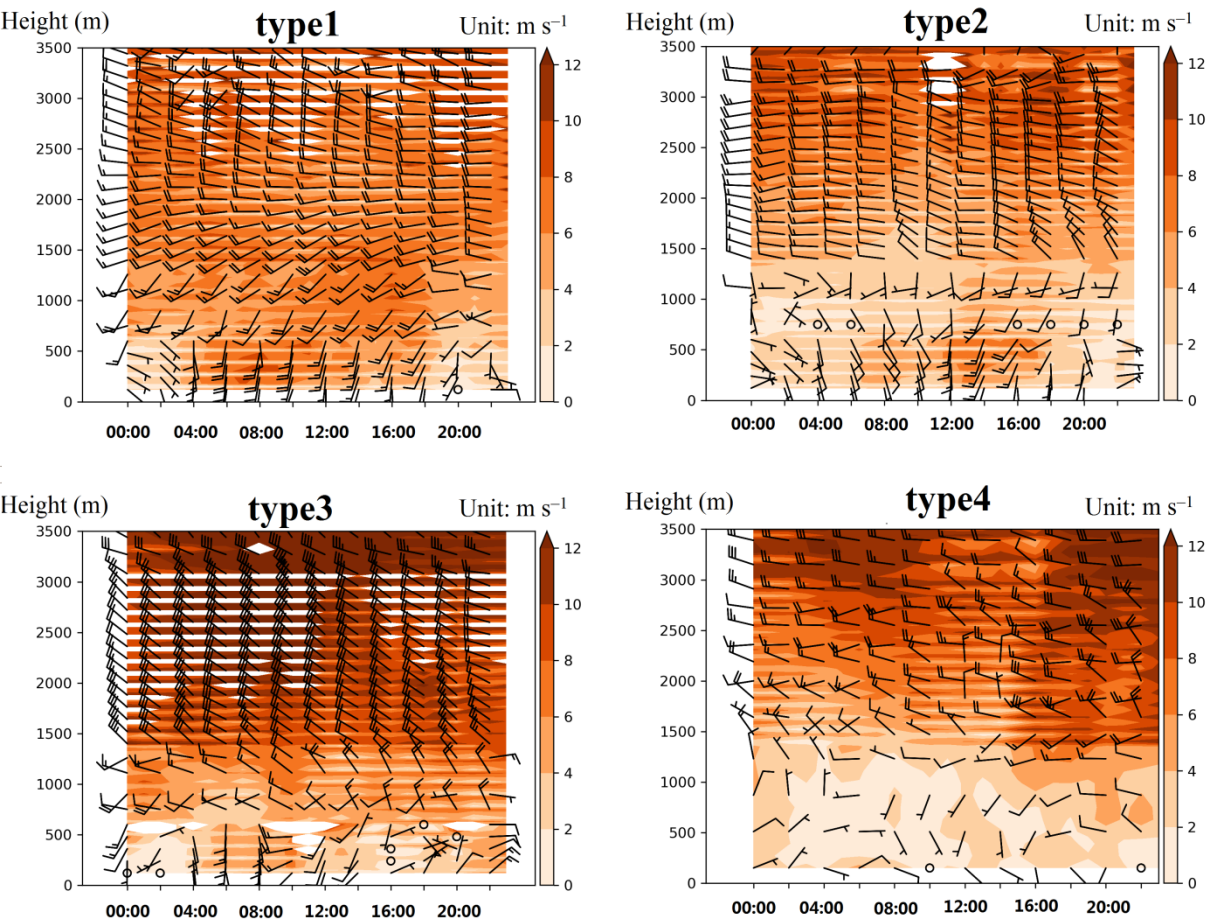
Figure 4.The mean wind field characteristics of the four pollution weather types in the Beijing Observatory (39.93°N, 116.28°E) (varying colors, based on the color bar to the right of each panel, represent the wind speed in m s^{-1}; the x-axis is in Beijing time from 00:00 to 23:00; the y-axis is the height in m).

667
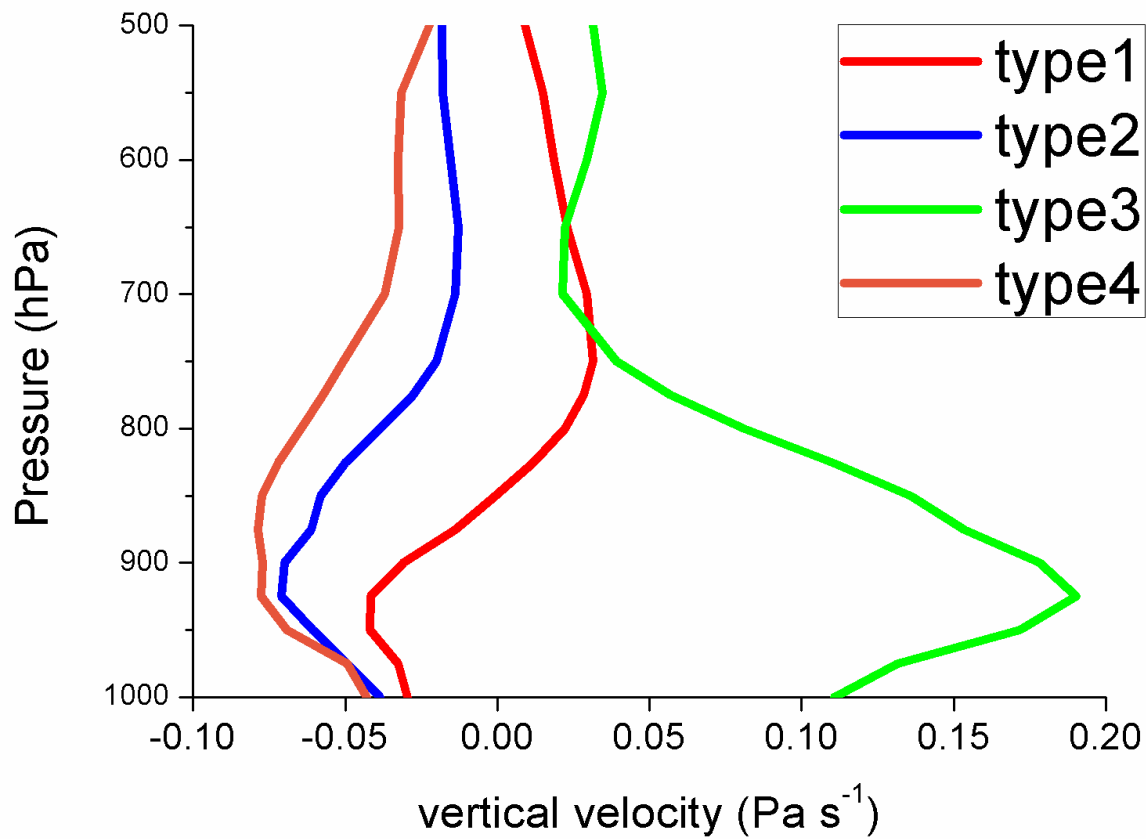
Figure 5.The vertical speed profiles in the four pollution weather types (type1: red, type2: blue, type3: green, and type4: red) in the Beijing Observatory (39.93°N, 116.28°E). The negative values represent ascending motion while positive values represent descending motion under the P coordinate(unit: Pa s^{-1}).

671

672

673

674
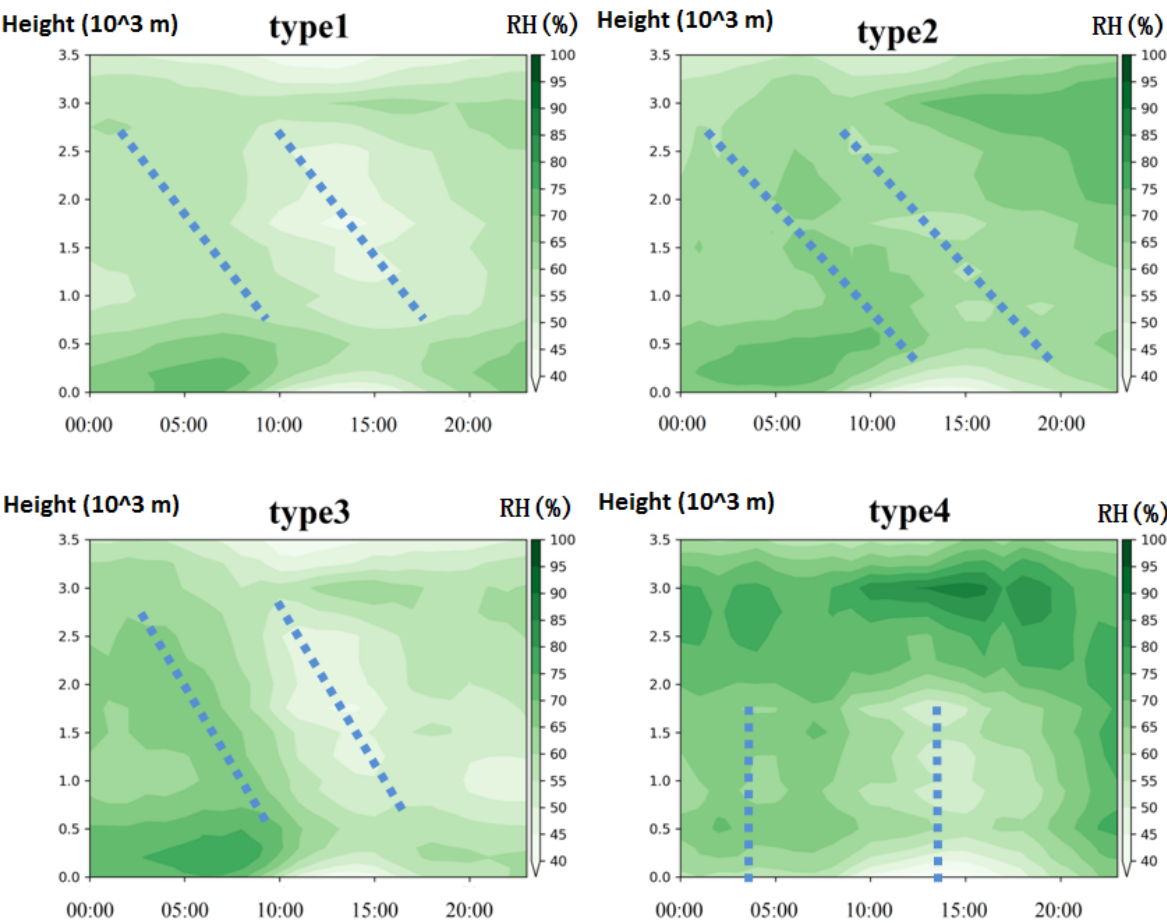
675 Figure. 6 Average characteristics of the relative humidity (RH) field in the boundary layer under four pollution types in the

676 Beijing Observatory (39.93°N, 116.28°E) (shadow represents relative humidity, unit:%; x-axis is Beijing time, from 00:00 to

677 23:00; y-axis is height, unit: km).

678

679

680

681

682

683

684

Figure 7.A thermodynamic and dynamic structure conceptual model of the pollution boundary layer for the four types of weather in the Beijing area. Arrows represent wind directions at different heights. Hollow arrow represents the ground horizontal wind field, thin red and blue arrows represent wind fields at different heights, and thick blue arrow represents the upper wind field. The dark red dots represent ground convergence lines, including 1) convergence between wind fields and 2) convergence between wind fields and topography. Solid red line is temperature. The Beijing area is located within the lowest rectangle, and the small figure in type4 represents mountain–plain winds with a daily cycle

691

692

693

694

695

696

697

698

699 Figure 8. The four pollution weather types in Beijing area: (a) average daily PM$_{2.5}$concentration at 12 state-controlled
700 stations (unit: μgm^3), (b) average daily relative humidity at the Beijing Observatory (unit:%), (c) average daily visibility at
701 the Beijing Observatory (unit: m), (d) average daily wind speed at the Beijing Observatory (m s^{-1}), and (e) the boundary
702 layer height from the tower station at the Institute of Atmospheric Physics, Chinese Academy of Sciences (unit: m).
703
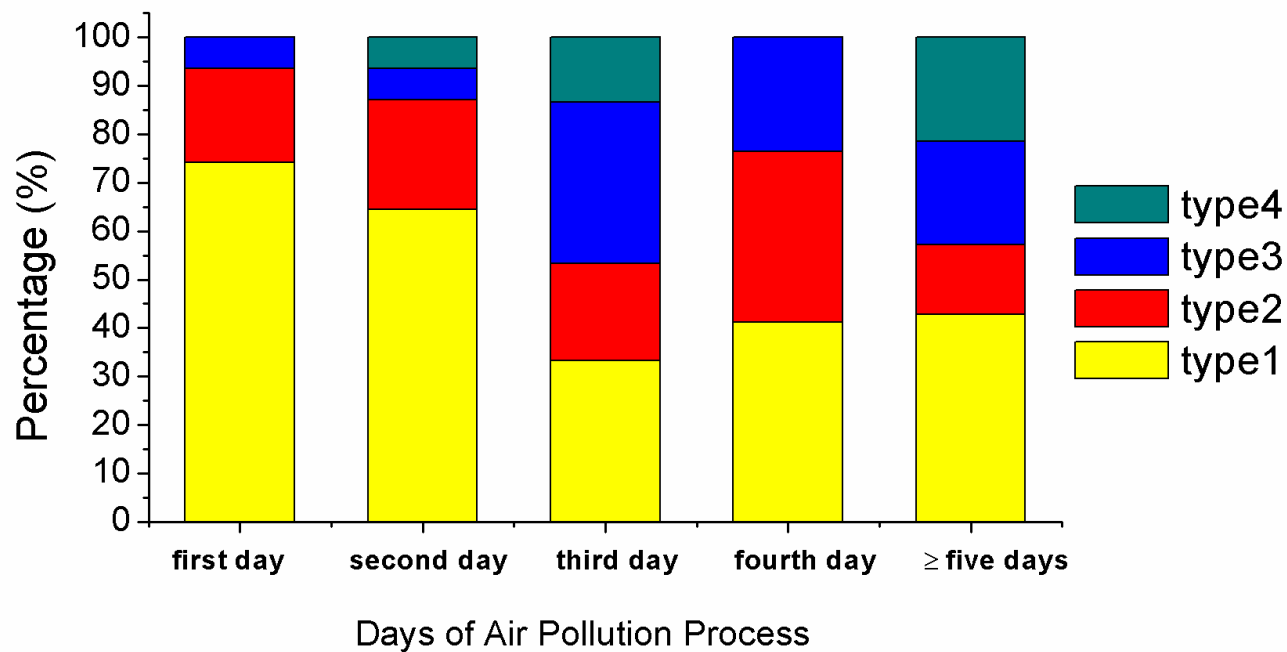
707 Figure 9. Time distribution of the four pollution weather types (yellow, red, blue, and green represent type1,type2,type3, and
708 type4, respectively) during pollution events in the Beijing area.

710

711

712
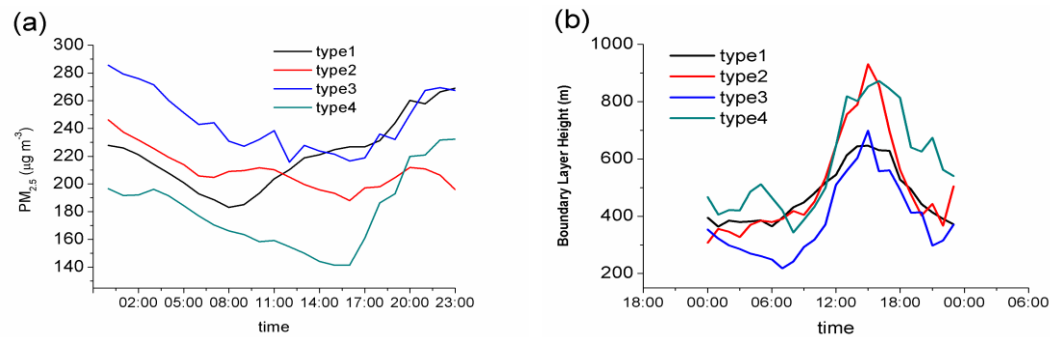
Figure 10. Diurnal variation characteristics of the (a) PM$_{2.5}$ averaged concentration (µg m^{-3}) and (b) boundary layer height
(m) under the four pollution weather types in the Beijing area(39.974°N, 116.372°E,) (x-axis: 00:00–23:00Beijing time).

715

716

717
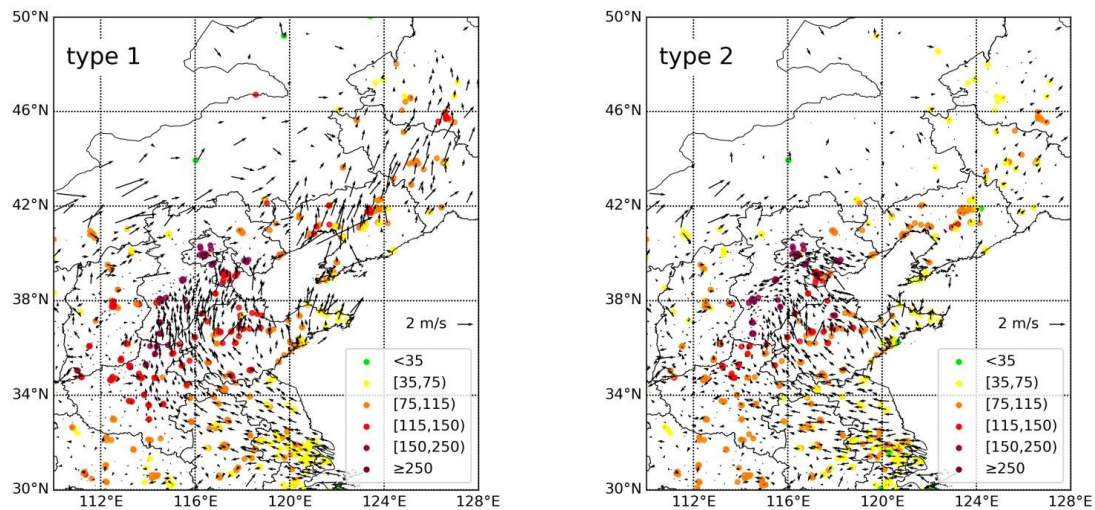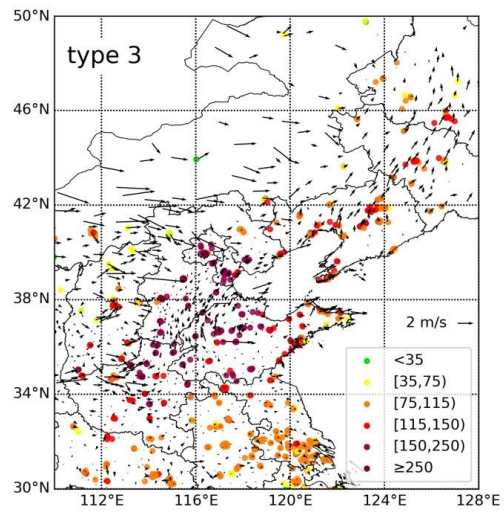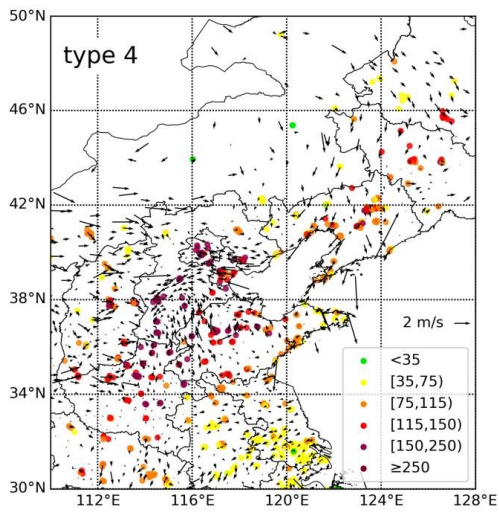
718   Figure 11. Spatial distribution of the PM$_{2.5}$ concentration (unit: μg m^{-3}) and wind field near the ground.
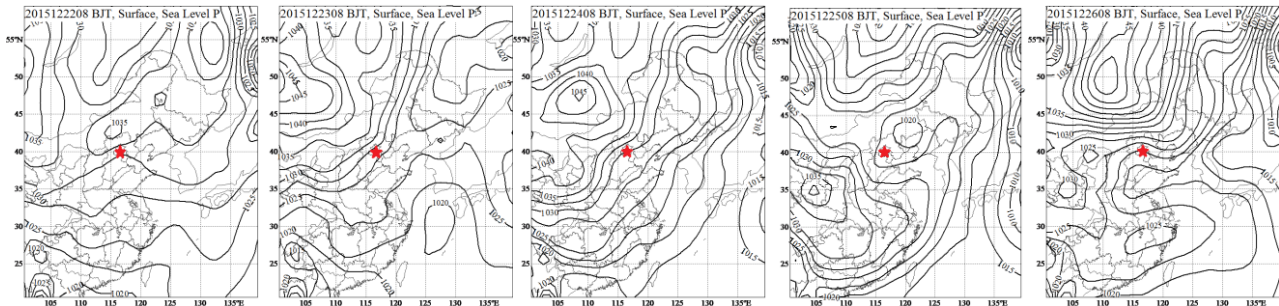
719

720

721

723

724

725

726
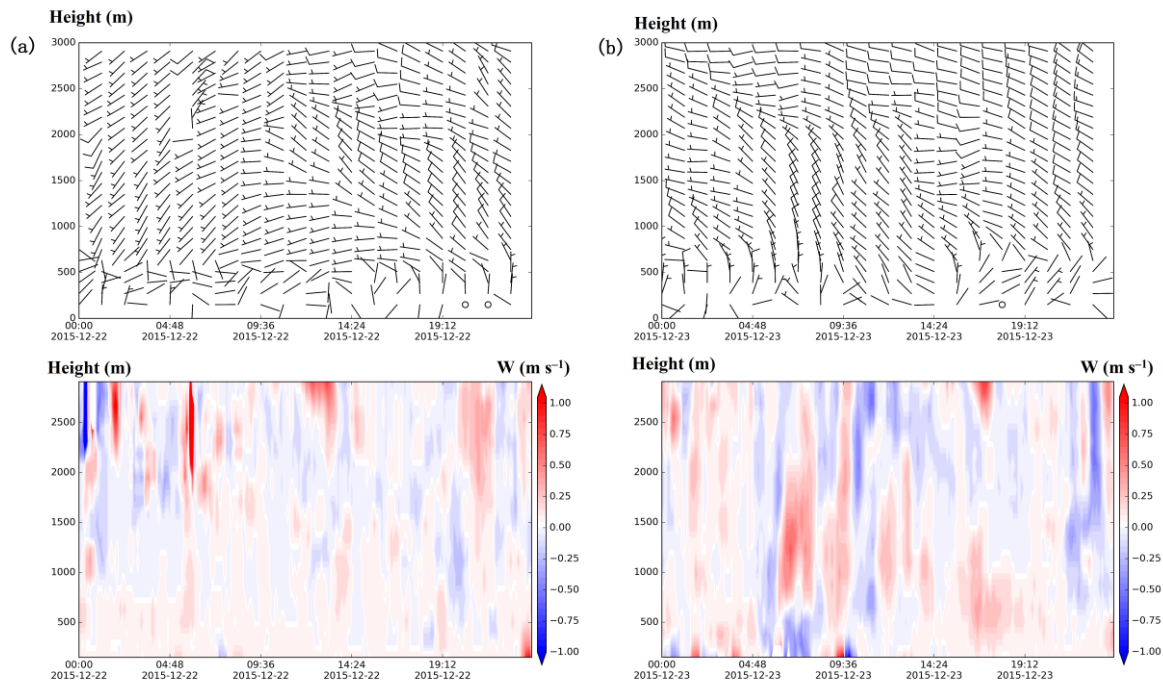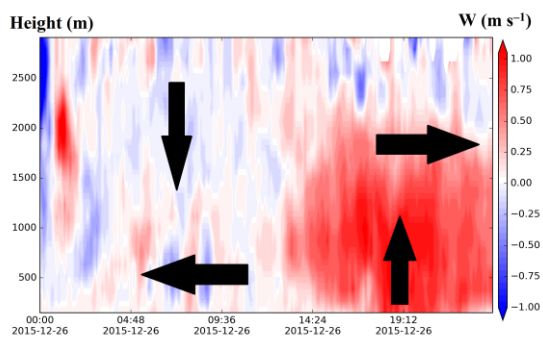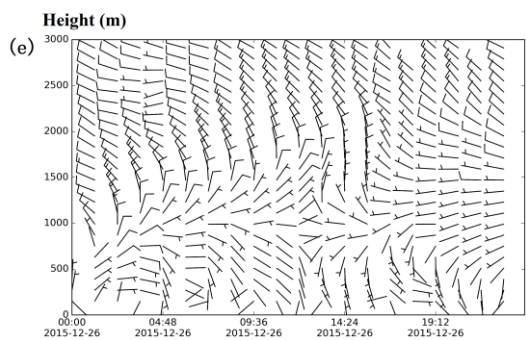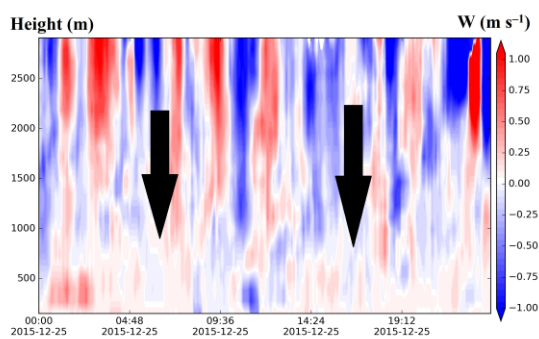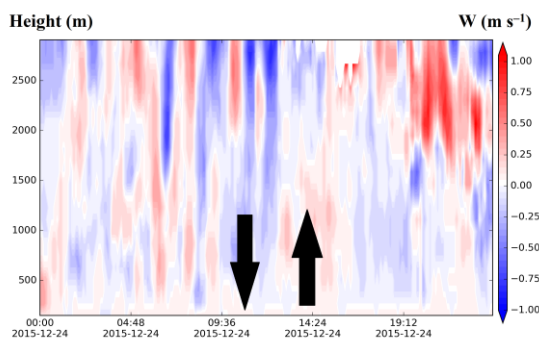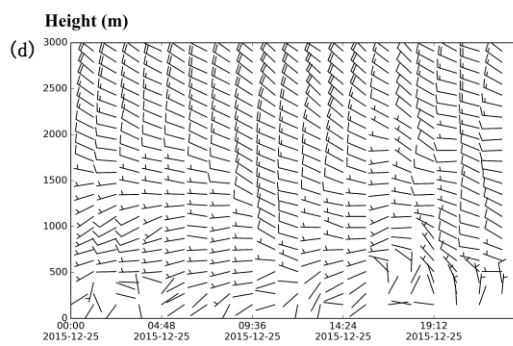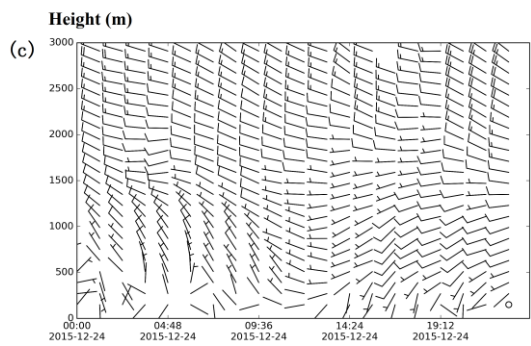
728 Figure 13.The horizontal and vertical wind field characteristics in the Beijing Observatory (39.93°N, 116.28°E) from

729 December 22 to 26,2015 (a-e,above is the horizontal wind field, below is the vertical wind speed (W), represent the wind

730 speed in m s^{-1},while red shadow represents the upward movement. The blue represents the sinking movement; the x-axis is

731 in Beijing time; the y-axis is the height in m).
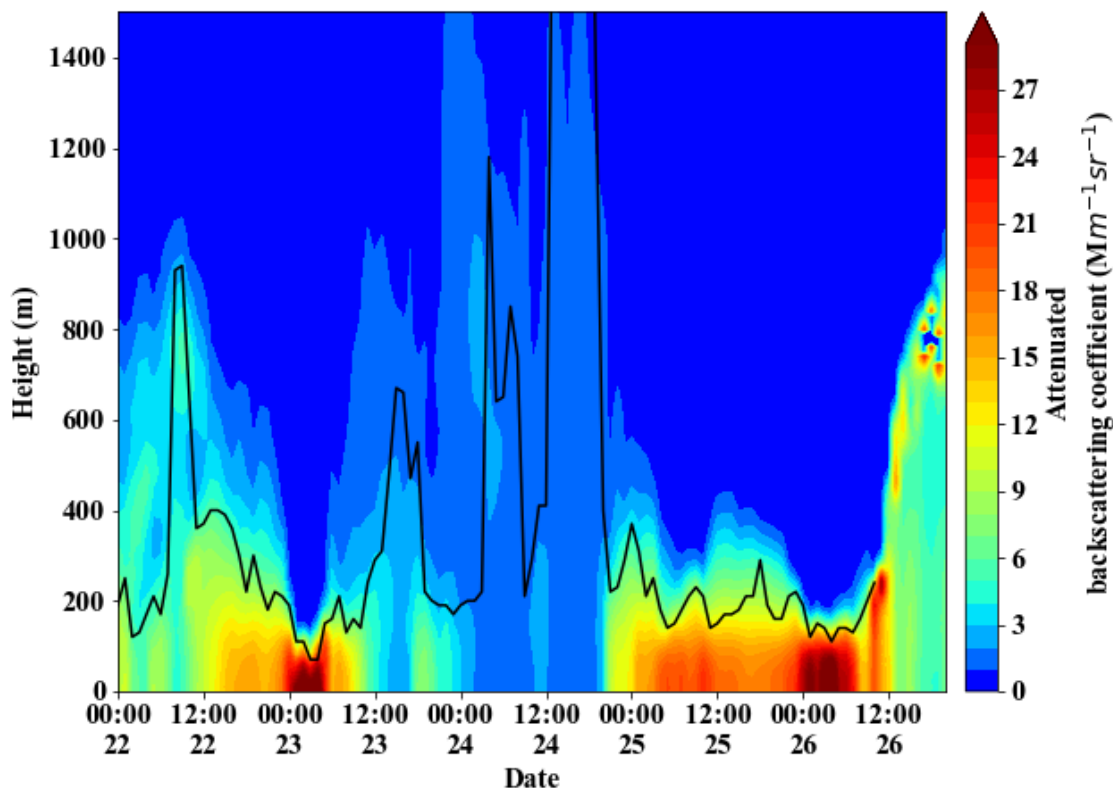
732

733 Figure 14. Aerosol backscattering intensity(Mm^{-1} sr^{-1}) from December 22 to 26,2015 in the Beijing area(39.974°N, 116.372°)

734 (y-axis is height in m and the x-axis is Beijing time).

735

736

737
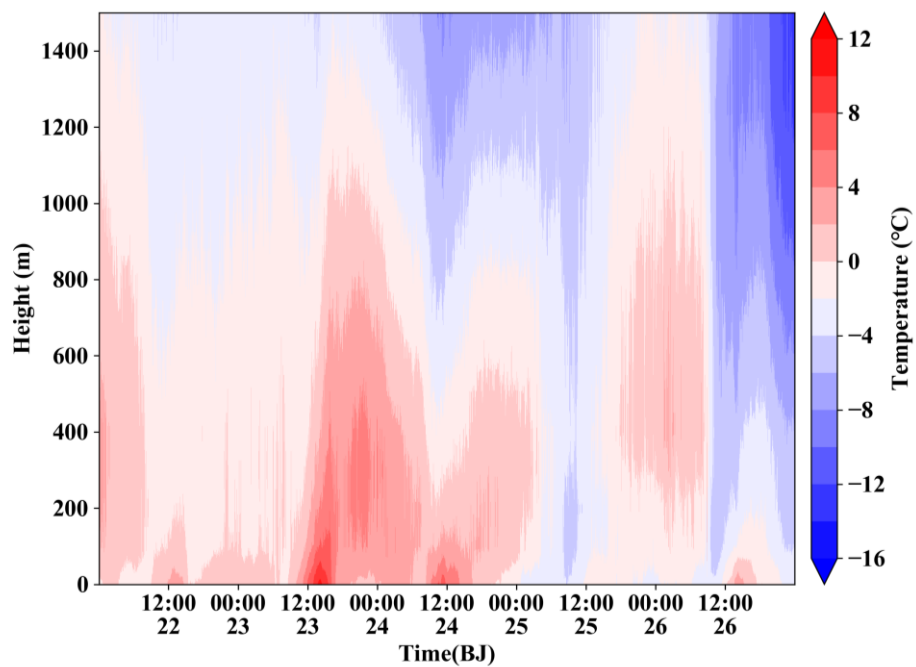
Fig. 15. Vertical temperature profile of Beijing from December 22 to 26,2015 in the Beijing Observatory(39.93°N,
116.28°E) (unit: °C).

740

741
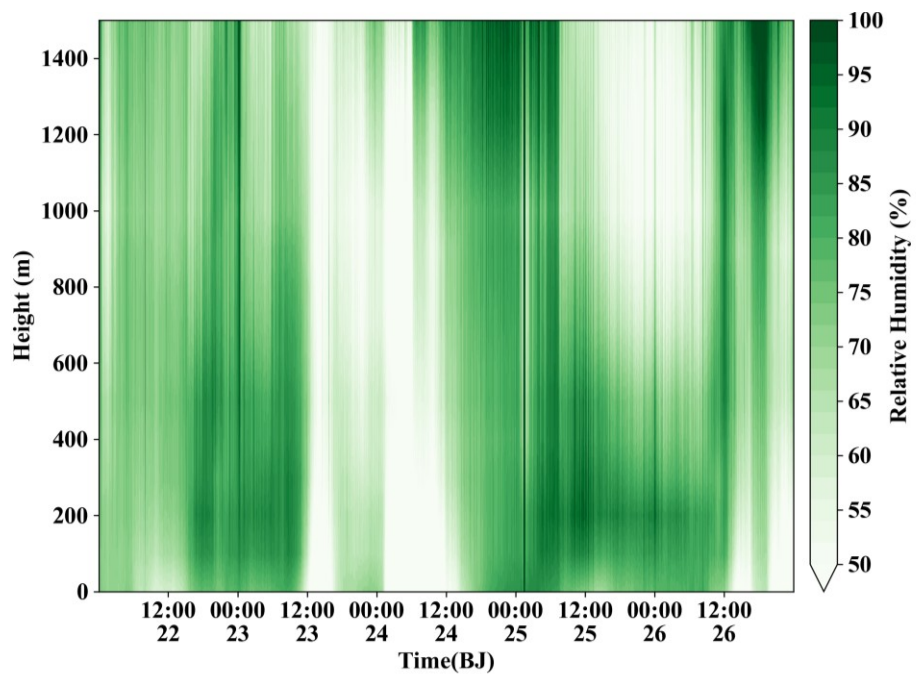
Fig. 16. Vertical relative humidity profile of Beijing at 08:00 and 20:00 BJT from December 22 to 26,2015 in the Beijing Observatory (39.93°N, 116.28°E) (unit:%).